Defect Detection via THz Imaging: Potentials and Limitations

by

Kaveh Houshmand

A thesis
presented to the University of Waterloo
in fulfillment of the
thesis requirement for the degree of
Master of Applied Science
in
Systems Design Engineering

Waterloo, Ontario, Canada, 2008

I hereby declare that I am the sole author of this thesis. This is a true copy of the thesis, including any required final revisions, as accepted by my examiners.

I understand that my thesis may be made electronically available to the public.

Abstract

Until recent years, terahertz (THz) waves were an undiscovered, or most importantly, an unexploited area of electromagnetic spectrum. This was due to difficulties in generation and detection of THz waves. Recent advances in hardware technology have started to open up the field to new applications such as THz imaging. This non-destructive and non-contact imaging technique can penetrate through diverse materials such that internal structures, in some cases invisible to other imaging modalities, can be visualized.

Today, there are variety of techniques available to generate and detect THz waves in both pulsed and continuous fashion in two different geometries; transition, and reflection modes. In this thesis continuous wave THz imaging was employed for higher spatial resolution.

However, with any new technology comes its challenges; automated processing of THz images can be quite cumbersome. Low contrast and the presence of a widely unknown type of noise make the analysis of these images difficult. In this work, there is an attempt to detect defects in composite material via segmentation by using a Terahertz imaging system. According to our knowledge, this is the first time that this type of materials are being tested under Terahertz cameras to detect manufacturing defects in aerospace industry.

In addition, segmentation accuracy of THz images have been investigated by using a phantom. Beyond the defect detection for composite materials, this can establish some general knowledge about Terahertz imaging, its capabilities and limitations.

To be able to segment the THz images successfully, pre-processing techniques are inevitable. In this thesis, a variety of different image processing techniques, self-developed or available from literature, have been employed for image enhancement. These methods range from filtering to contrast adjustment to fusion of phase and amplitude images by using fuzzy set theory, to just name a few. The result of pre-procssing and segmentation methods demonstrates promising outcome for future work in this field.

Acknowledgements

I would like thank my supervisor, Dr. Hamid R. Tizhoosh, for all the assistance and guidance he has provided me over the past two years. He has helped me with open arms at anytime of the day, during my research and writing.

I would like to thank Dr. Karray, and Dr. Kumaraswamy for offering their time to read this thesis.

I would like to thank *Pratt & Whitney Canada* for their generous grant for my research, and specially Mr. David Craig for providing me the samples for this research and his continuos efforts for using THz imaging in aerospace industry.

I would like to thank Professor X.-C. Zhang and Dr. Albert Redo-Sanchez for their support at Rensselaer Polytechnic Institute (RPI). Their hospitality at Troy, NY, was collegial and pleasant.

I would like to thank my parents (Fantaneh, and Sirous) for their support. Anytime I was down during this time, i knew where to go for warming help. They have done anything they could in my life.

I would like to thank my aunt (Rezi) for her support during the last two years, and my grand mother (Maman LyLy) for her continuous support.

Finally, I would like thank my friends who have been there for me since my undergrad.

Cogito, ergo sum – I think, therefore I am

Ren Descartes

To my grand father, Dr. Mehdi Houshmand, whom was the inspiration of my life

Contents

List of Tables

List of Figures

Chapter 1

Introduction

In this chapter, the reader will be introduced into Terahertz technology and defect detection in composite materials. As well, a brief overview of thesis will be provided.

1.1 Background on Terahertz Technology

Terahertz (THz, T-ray) region within the electromagnetic spectrum has become available with the recent development in semi-conductor technology and ultra-fast lasers [2]. These type of lasers made the Terahertz endeavor possible for the region of the electromagnetic spectrum previously known as the "terahertz gap" as shown in Fig. 1.1. This growing technology is rapidly flourishing due to the fact that THz systems are non-destructive and contact-free detection techniques with some advantages over existing technologies such as X-ray and thermal imaging.

The THz wavelength interval ranges between the top edge of the millimeter wave spectrum to the bottom edge of the optical spectrum, corresponding to the boundary of the far-infrared (FIR) region. The advancement in laser technology and developing techniques such as optical rectification and difference frequency generation for production of THz radiation, have significantly increased the applicability of this novel technology over the past years [2].

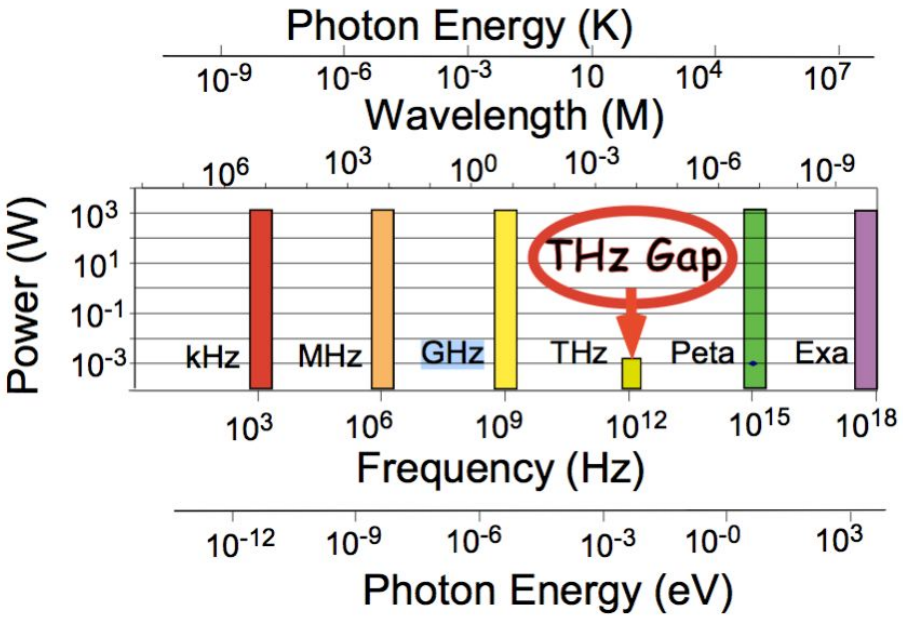

Figure 1.1: The electromagnetic spectrum with the "terahertz gap" [source: [8]]

Terahertz waves are abundant in nature, however, it was impossible to coherently generate and detect this type of waves until the late 1980's [1]. This gap between 'electronic' and 'photonic' regions is very interesting for several reasons. Firstly, for generation, detection, and processing of THz waves, both electronic or optical, or even mixture of optical and electronic techniques can be employed [3]. Also, this range of waves are extremely sensitive to polar substances, such as water, and insensitive to non-polar substances such as dust, plastic, leather, wood, and fabrics. These materials are almost transparent under T-rays which means THz imaging could be employed for quality control via analysis of their internal structures.

It was not until 1995 that THz technology was used for imaging purposes [2]. This work provoked a lot of interest in many application fields. To be able to form images in a reasonable time, combined with the unique properties of THz radiation, these developments opened up new doors for applications ranging from biomedical diagnosis to security purposes to quality control applications [2]. These applications range from pharmaceutical analysis for finding coating integrity in tablets [10] to defect detection in composite material for air-

space industry, which will be discussed in this thesis. These are just a few applications to name in a broad range of applications in this field.

Fig. 1.2 displays two samples of THz images to demonstrate the unique capabilities of this technology. The first one shows how the inside content of a leather bag has been revealed. THz radiation successfully penetrated though the bag and the items are vivid to the viewer. The second sample shows the inside of an air-freshener. THz waves have gone through the air-freshener without any problem. These examples illustrate how these systems could be very useful for security purposes which seems to be a very attractive application to many researchers [13].

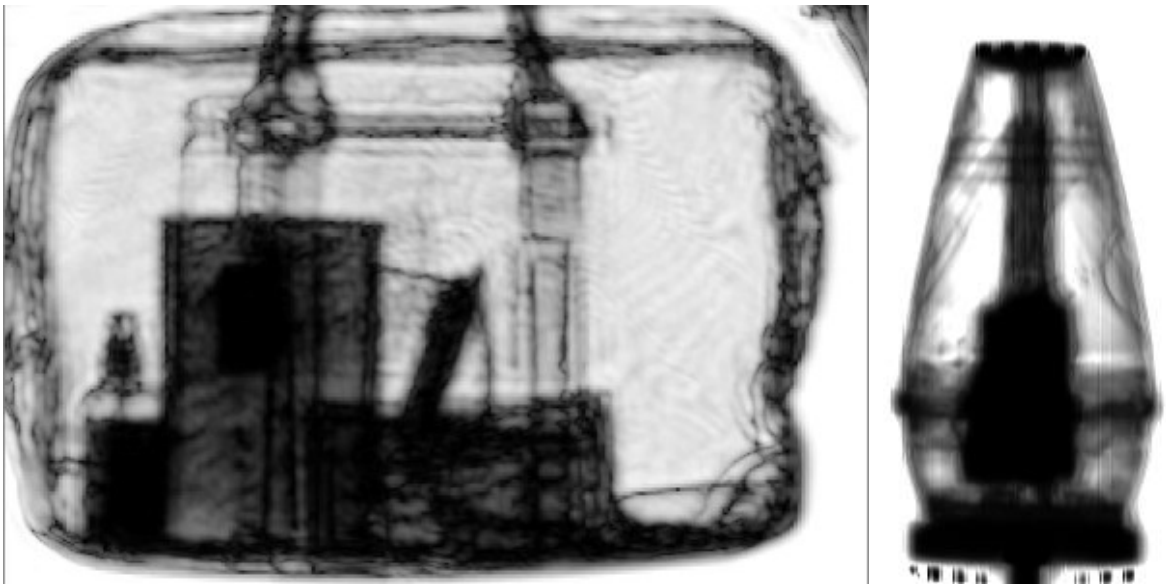

Figure 1.2: Sample THz images. Left: inside a leather bag, right: image of an air freshener [Source: Terahertz Research Center, RPI]

1.2 THz imaging: Defect Detection

A THz image can be formed by measuring the transmitted or reflected THz waveforms for each position of the object. This image can be in any form of measured aspect of the waveform: the amplitude [5], phase or any combination of the two [6] [7]. This versatility

provides flexibility for different applications, because each image could represent different properties of the sample under investigation [2].

There are many applications for such a system with these properties. Perhaps one of the most promising applications is in quality control of different materials. In this thesis, the fusion of phase and amplitude images has been used to find defects in composite materials. This material, which is provided by Pratt & Whitney Canada has a very dense molecular structure, as a result very hard to penetrate through them for many imaging techniques (e.g. ultrasound and thermal imaging). As far as its known, this is the first time that these materials were exposed to THz waves for defect detection in aerospace industry. Therefore, a wide range of frequencies were tested to localize the ideal frequency for this type of material.

Delamination is a mode of failure in composite material. This phenomena occurs after repeated cyclic stresses on the material. The material starts to separate and form a mica-like structure. This causes notable loss in mechanical toughness, and could be fatal in the industry. Therefore, it is crucial to be able to segment the images and pinpoint the delamination in the composite material. To attain effective segmentation results, intelligent pre-processing techniques are essential. In this thesis, combination of different pre-processing techniques were employed for defect detection in composite materials.

In addition, since non-polar substances such as cardboard and plastic are transparent to THz waves, phantom objects were used to measure the spatial accuracy of the THz imaging. A phantom with 41 circles on a plastic material was placed inside of two cardboard. Hence, the THz waves could easily penetrate through this material and segmentation accuracy measurement could be achieved. Segmentation without pre-processing is meaningless for THz images. Consequently, in this thesis a variety of pre-processing techniques from literature have been used. In addition, several new techniques have been developed to customize the processing.

1.3 Overview of Thesis

In this thesis, the rapid advancement in THz technology will be briefly explained in Chapter 2. In addition, different types of generation and detection of Terahertz waves will be elaborated on in this chapter, and diffrent types of imaging will be discussed. Furthermore, different image processing techniques, which will be employed to obtain optimal results will be explained in Chapter 3. Terahertz images are generally quite challenging for segmentation due to a low signal to noise ratio (SNR) and lack of information on what type of noise these images contain. Therefore, pre-processing techniques are necessary before segmentation. These techniques are mostly filtering methods and contrast adjustment techniques to improve the SNR ratio. All the result from preprocessing and segmentation of the THz images will be presented in Chapter 4. Finally, Chapter 5 will conclude the thesis with pointing to some future works.

Chapter 2

Terahertz Imaging: An Emerging Technology

Terahertz waves belong to the part of the electromagnetic spectrum between the far infrared and microwave regions. This region has been historically underdeveloped in comparison to the neighbouring regions of microwave and infrared, despite the fact that it has been subject of interest for scientist since the early discovery in 1897 [9]. This is mostly because of lack of suitable techniques for radiation detection and generation. However, recently with the advances in semi-conductor technology, new sources have been discovered and the hardware development in this field has experienced a considerable boom.

Some researchers consider THz waves to range from 100 GHz up to 10 THz. Although, strictly speaking, THz waves are those with frequencies between 1 to 10 THz. Terahertz frequencies range from 3 mm (100 GHz) up to 30 μm (10 THz) . This wavelength interval ranges from top of millimeter wave spectrum to the bottom edge of the optical spectrum [3].

Other facts about terahertz technology can be summarized as follows [1] [11] [12]:

- Terahertz radiation is non-ionizing, which means that they are completely harmless to living tissues
- The wavelength is shorter than microwave, with the associated improvement in spatial resolution, while still being long enough to experience less of the Rayleigh scattering

experienced by infrared

- Light weight molecules have strong emission or absorption lines in this region for rotational and vibrational excitations
- Terahertz waves are very sensitive to polar substances such as water, and extremely insensitive to non-polar substances such as plastic, fibers etc.
- The universe is naturally bathed in Terahertz radiations

It was difficult to efficiently detect and generate THz waves until recent years. In the past, most THz sources were thermal sources, which are very low-brightess emitters, or single frequency molecular vapor lasers [4]. To understand the novelty of this technology it is important to take a look at the history of THz in general and THz imaging in particular, which is the main topic of this thesis.

2.1 THz Technology: A Historic Perspective

Electromagnetic radiation in terahertz region was first obtained by Heinirich Rubens in 1897 [9]. However, it remained unexplored in the following years. This region was known as "terahertz gap". This was as a result of the fact that optical techniques could not operate below a few hundred terahertz. Also, electronic methods could not operate above a few hundred gigahertz [3].

Many techniques have been proposed in recent years for detection and generation of FIR (Far Infrared) light, many of which relied on nonlinear optical techniques. The first development in FIR region using non-linear optical techniques was proposed as early as 1976 by Y.R Shen in a paper called "Far-infrared generation by optical mixing" [15]. Shen did his work with limited laser capabilities. With the rapid advances in laser technology, new techniques were developed in this field. One of the earliest methods that was proposed was Terahertz time domain spectroscopy (THz-TDS). By using ultra-fast laser pulses, this method generates coherent terahertz waves and was established, in the late 1980's, by research groups at

AT & T Bell Laboratories [2] and IBM's T.J Watson Research Center [2]. The advantage of coherent detection is to record the amplitude of the electric field in the time domain. This way Fourier transforms, wavelet transforms, and other time/frequency techniques can be used for analysis.

The next step was to build an imaging system using the terahertz time-domain spectroscopy. The first effort was done by Van Exter et al. in early 1990's [16]. The first real time terahertz pulsed imaging system was reported in 1995 by Hu an Nuss [5]. This work has sparked a lot of interest in many fields, and in the pubic media. Therefore, many companies start to invest in the technology. As a result, the first commercially made THz-TDS system, which was a pulsed imaging system, was developed in early 2000 [17]. However, these systems were really expensive and bulky.

Today, there are many systems available in both pulsed and continuous wave (CW). Continuous systems [18][19] use monochromatic radiation that can be tuned to specific frequencies. CW images were first captured by Siebert et al., [20], using a two colour Ti: sapphire laser. The system worked at room temperature and with a signal to noise ratio (SNR) of around 100:1. However, this type of laser was very complex and expensive. Kleine-Ostmann et al. [18] have developed an imaging system using a two-colour external-cavity laser diode. They presented images of biological tissue, with a SNR of around 75:1. They achieved improvements in SNR, but detection was achieved using a bolometer. This type of detection needs cryogenic cooling, and severely limits the modulation bandwidth. This work led to a new wave of research projects in THz technology. Today, there are many methods available to generate and detect CW waves including gas lasers, photomixing of two diode lasers, and quantum-cascade laser (QSL) to name a few [23] [25] [30] .

2.2 Terahertz Imaging

There are two type of Terahertz imaging, continuous and pulsed. In both cases, broadband Terahertz pulses or continuous waves are generated, steered to interact with the sample and captured either in the *transition* or in the *reflection* mode. In *transition mode*, the

detector is on the other side of the sample to detect the waves. In *reflection mode*, the detector is on the same side as the sample, as the transmitter being positioned in such way to capture reflection from the sample [1]. In this thesis the images were captured using THz continuous-wave (CW) source, in both transition and reflection geometries.

At the beginning of the THz era, the feasibility of THz imaging with pulsed system was demonstrated [27]. Development of continuous systems, and also quantum cascaded lasers, opened up new doors for THz imaging. While THz pulsed imaging has the advantage of providing an image with broad frequency information between 0.1 and 5 THz, the advantage of continuous-wave THz imaging lies in the fact that it has higher power spectral density [29]. The problem with these systems is the difficulty of achieving high output-power for higher frequencies. The highest output power accomplished has been reported by Japanese researchers [21]. They reported to have attained 30 mW at 3.1 THz with quantum cascade lasers. This is quite high at that frequency. These lasers work in such a way, which photon generation takes place via electronic intersubband transitions in semiconductor heterostructures [22] [23]. However, in lower frequencies higher output power can be reached easier.

In this thesis, the commercially available SIFIR-50 FPL THz gas laser was used to obtain some of the images. This device has its highest output power at 1.63 THz with an output power of 181.5 mW. Higher output power generally means better spatial resolution.

2.2.1 Terahertz Pulsed Imaging: THz-TDS

In Terahertz pulsed imaging, ultrashort optical pulses can be generated using non-linear optics or a dipole antennas. These pulses are directed to interact with a sample, and are observed in time domain afterwards. A typical THz imaging setup is shown in Fig. 2.1 [14].

The system has two photoconductive dipole antennas which are used for emitting and detecting THz pulses. The pulses are produced by $Ti : Al_20_3$ laser with a repetition rate of 80 MHZ [14], the pulses can be delayed if necessary with two optical delay lines. Short electrical pulse is generated when an optical pulse hits the emitter antenna. Maxwell's law

states emitted electromagnetic field is given by the derivative of its current spike. As a result, the emitted electromagnetic field has strong components in the THz region if the electric pulse rises fast enough [24]. Then these waves interact with the sample in raster scan fashion, and the transmitted waves are focused into the detecting antenna. Using this technique, THZ waves can be detected. A sample of THz waveform is displayed in Fig. 2.2 [14]. Using the Fourier transform and spectral integration over a certain range for these waves, images can be captured in pixel form.

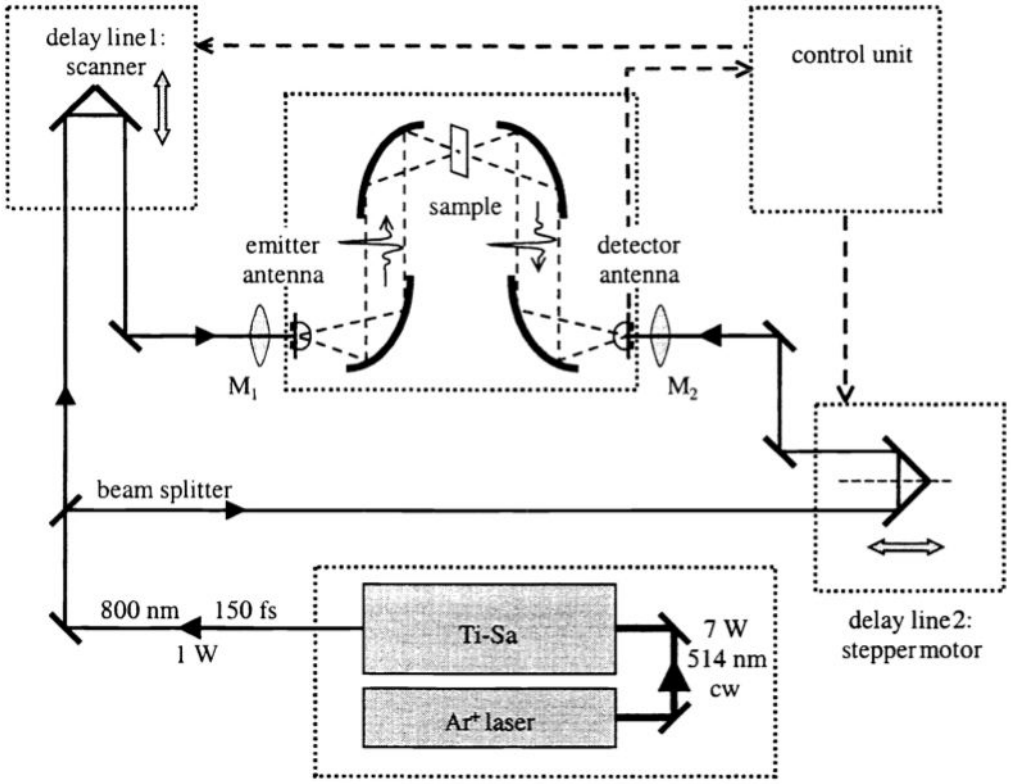

Figure 2.1: THz-TDS imaging setup [source: [14]]

2.2.2 Continuous-Wave Imaging

There are many ways to generate and detect CW waves. Since in this thesis a gas laser was used to capture most of the images, the focus of this section is to provide more information

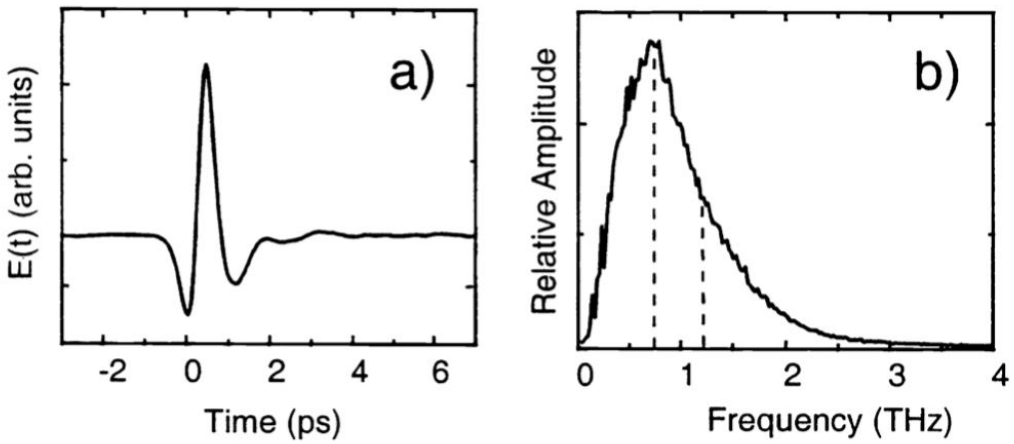

Figure 2.2: THz waveforms: a) typical THz TDS waveform, b) Fourier transform of the waveform [source: [14]]

on these systems. Other popular systems are photomixing of two diode lasers and quantum cascaded lasers.

By photomixing of two diode lasers in a photoconductor continuous wave THz can be produced. The difference in the frequency of the two lasers are tuned to the THz region. This way, monochromatic CW-THz is emitted at the beat frequency by using two diode lasers. A DC current is detected, when the THz radiation and the beat modulation arrive at the receivers in phase [30]. Also, by varying the optical path length to the receiver, both phase and amplitude information could be attained. Photomixing of two diode laser is shown in Fig. 2.3. Unfortunately, this method does not achieve very high output power, this means low spatial resolution. As a result, photomixing may not be suitable for imaging purposes.

Quantum cascaded lasers (QCLs) are another promising technology for THz source development. QCLs are semiconductor devices originally proposed by Kazarinov and Suris [32] and first developed by Faist et al. [33] in the mid-infrared region and Kohler et al. [23] in the terahertz region. In QCLs, light emission is produced through intersubband transitions in the quantum wells. Light emission occurs through the intersubband transition between the upper and lower laser states [21]. Afterwards, electrons are removed by an extractor

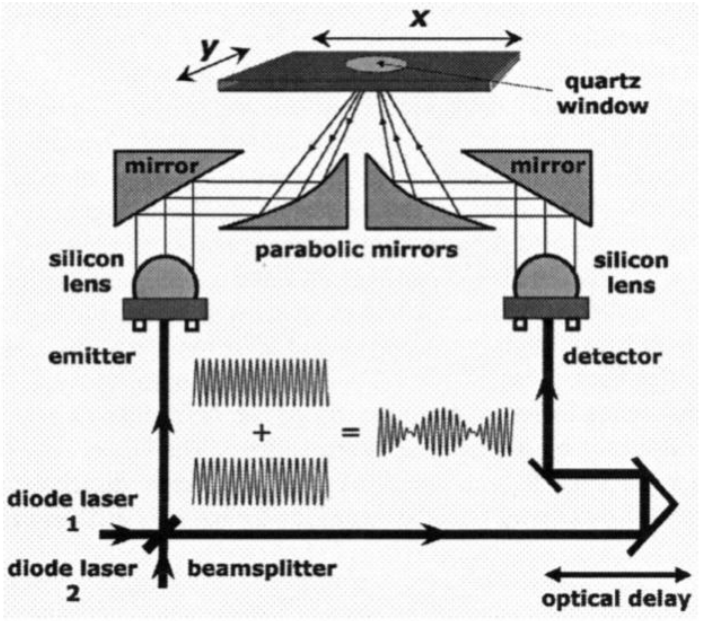

Figure 2.3: Photomixing of two diode lasers to attain CW THz waves [source: [31]]

and then fed into the next active part by resonant tunneling. This method produces higher output power, however, they require cryogenic cooling, which prevents this systems to be compact and portable. Also, these systems are very expensive due to complex manufacturing process.

In this thesis, a method with a reasonable cost and output power for imaging was chosen. This method is the gas laser. In a gas laser source, a CO2 laser pumps gas with a low pressure into the gas cavity (FIR cavity). This way it emits radiation at its emission-line frequencies that lie within the THz range.

Gas lasers can provide a broad range of frequencies with a power from few to hundred mW [25], and are tunable to distinct lines by varying the composition and pressure of the gas in the laser cavity and the frequency of the CO2 pump laser. The CO2 laser [27] is grating-tuned and its emission lies between 9 and 11 μm. This radiation is introduced inside the FIR cavity through a small coupling hole in one end-mirror and the THz radiation produced is emitted through another coupling hole in the other end-mirror.

The THz laser process operates on the molecular rotational transitions of the low pressure

gas. In the actual system, CH3OH, CD3OH and CH2F2 gases are available. An infrared photon generated by the CO2 with energy close to a transition from a particular rotational ground state to a rotational excited state is absorbed by a gas molecule. If the population inversion is achieved, the molecule decays through different rotational excited states to the ground state and emits laser radiation according to the energy difference of these excited states. Fig. 2.4 illustrates how methanol can excite the molecules to produce terahertz waves.

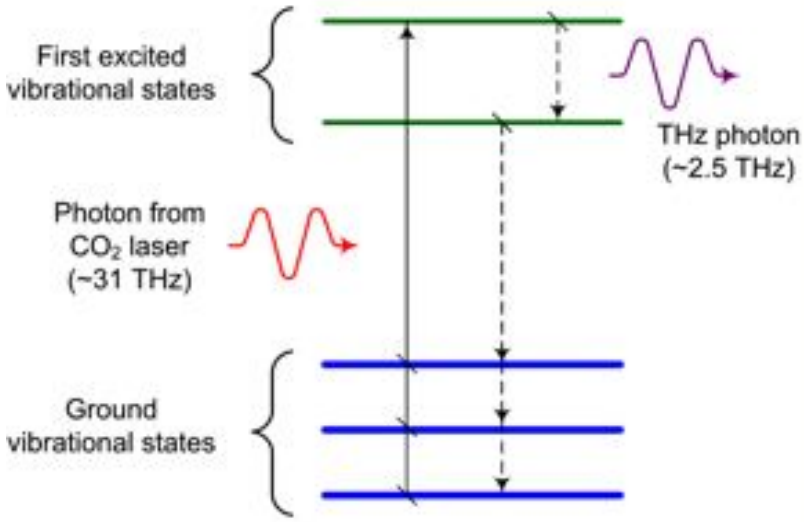

Figure 2.4: Laser process using methanol (CH3OH) as the emission gas [Source: Terahertz Research Center, RPI]

Subsequently, the emitted THz beam is brought to a focus on a horizontal imaging plate using parabolic mirrors. Automated motors are used to move the sample in the desired (x,y) direction. For detection, the output signal, either in reflection or in transmission mode, is fed to a lock-in amplifier.

Below, SIFIR-50 FPL THz gas laser components are shown in Fig. 2.5-2.7. In addition, all available THz frequencies are displayed in Fig. 2.8:

Figure 2.5: Front panel of the SIFIR-FPL system controller. Some main components: main power key (1), green on button (2), red off button (3), pump laser RF ON switch (4), frequency offset knob (6), pump PZT (7), loop control knob (8), FIR PZT (9), pump shutter(10) [Captured by author in Terahertz Research Center, RPI]

2.2.3 Noise in THz Images

Undesired data and the corruption of signals are usually classified as noise. Before removing the noise, it should be recognized and modeled first. The noise in Terahertz imaging can be split in to two categories: signal noise and imaging noise.

Signal noise has three main components; Johnson noise [28], shot noise, and set-up noise [1]. We are not going to discuss these forms of noise any further, because we only work with the images.

Imaging noise, on the other hand, is a noise that is introduced though the imaging acquisition process. This type of noise is present due to several reasons. Firstly, raster scanning errors can cause straight edges to appear staggered [1]. Furthermore, the motor moving the sample may not shift it correctly, leading to a varying physical distance between pixels on the image. Also, the noise in the THz images depends on the application, some materials are much denser to get through and hence may cause a lot of noise due to, among

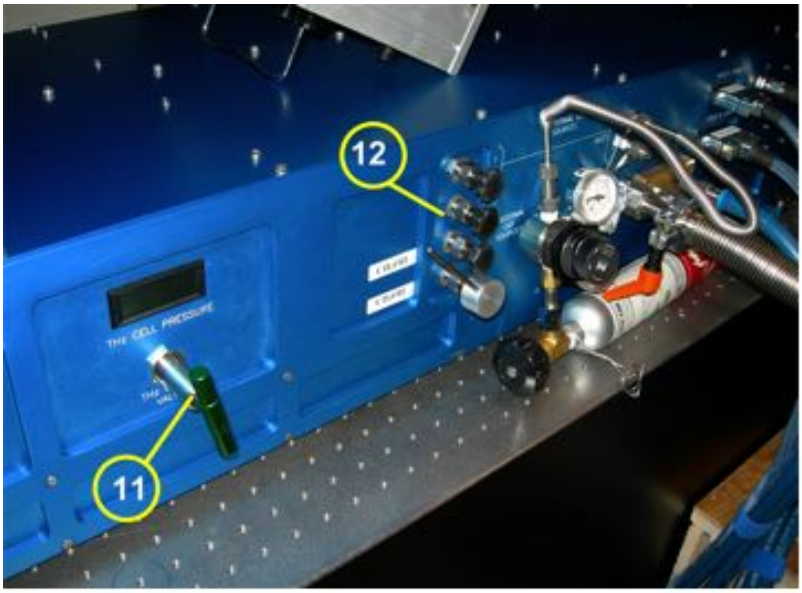

Figure 2.6: Vacuum (11), and gas valves (12) [Captured by author in Terahertz Research Center, RPI]

others, severe scattering. Different applications will be shown in chapter 4.

Furthermore, It is still not clear to scientists which type of imaging noise exists in THz images due to the novelty of the technology. As a result, this is going to be one of the major challenges in ongoing research in terahertz imaging.

2.2.4 Summary

Any novel technology transpires its own challenges. Scientist have accomplished notable success in the hardware of this emerging technology. The advances in the hardware have opened up the doors for imaging in this field . This way THz images can be utilize for many applications in the industry. To be able to use THz images, pre-processing techniques are necessary to remove the unwanted noise in these images. However, the noise in THz images are not well studied and it is not modeled as this is the case for other modalities. Therefore, in this thesis fundamental work has been done to be able to remove the extra noise and filter the images. Fortunately, after comprehensive research reported in literature, a few

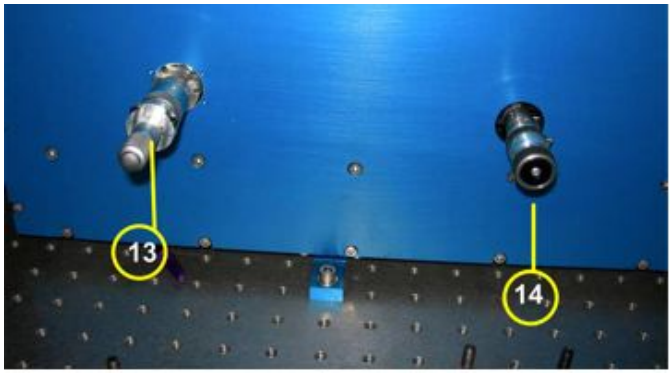

Figure 2.7: Pump grating control (13) and FIR laser cavity length control (14) [Captured by author in Terahertz Research Center, RPI]

edge preserving filters have been found in this thesis that have shown promising results for noise removal in THz images.

Freq. (THz)	CO_2 Pump line	Micrometer reading		Pol.(*)	Gas	Optimal Pressure (mTorr)	Power (mW)	FIR laser meter reading	
		Coarse	Fine					X1	X10
6.86	10R18	7.932	1.000	N	CD_3OH	280	2	0.08	0.54
5.67	9R34	6.530	0.290	P	CD_3OH	425	3.1	0.16	>1
4.25	9P34	7.040	1.000	P	CH_3OH	295	23.2	0.13	0.84
3.11	9R10	6.530	1.815	N	CH_3OH	575	18.8	0.34	>1
2.74	9P24	6.922	1.000	N	CH_2F_2	505	38.6	0.42	>1
2.55	9R20	6.530	1.143	P	CH_2F_2	510	61.3	0.13	0.84
2.52	9P36	7.065	1.000	P	CH_3OH	365	67.5	0.22	>1
2.45	9R22	6.530	0.990	P	CH_2F_2	490	60.8	0.18	>1
2.24	9P22	6.898	1.000	P	CH_2F_2	575	84.4	0.12	0.86
1.89	9P10	6.780	1.000	N	CH_2F_2	245	90.1	0.78	>1
1.63	9R32	6.530	0.410	P	CH_2F_2	245	181.5	0.2	>1
1.40	9R34	6.530	0.290	P	CH_2F_2	150	63.2	0.04	0.23
1.27	9R6	6.530	2.218	N	CH_2F_2	80	16.7	0.04	0.22
1.04	9R34	6.530	0.290	N	CH_2F_2	225	13.7	0.04	0.24

Figure 2.8: Operational parameters of the gas laser, (*Pol. means polarization: P is parallel to the horizontal surface and N is normal to the surface) [Source: Terahertz Research Center, RPI]

Chapter 3

Image Processing Techniques

In this chapter, a brief overview of image processing techniques will be provided which were employed to enhance and segment THz images in this project.

3.1 Introduction

Image segmentation is one of the most fundamental tasks in the field of image processing and is a crucial step in many applications, especially for industrial quality control and medical imaging. The objective of image segmentation is to partition the image and extract the region of interest (ROI) from the rest of the image. This thesis uses soft computing techniques such as fuzzy logic and different filtering methods to pre-process THz images. This step will prepare the images for image segmentation for several different applications. Terahertz images are generally challenging to segment due to a low signal to noise ratio (SNR). As well, the effect and type of noise in these images are widely unexamined due to novelty of the technology. Therefore, pre-processing techniques are necessary before segmentation. Besides, the research on THz technology has been widely focused on the hardware aspects neglecting the image processing challenges.

There are many different pre-processing techniques available in literature. In this thesis, some of these techniques that were applied to the THz images will be investigated. These

methods are sticks filter, Frost filter, Wiener filter, median filter, adaptive histogram equalization, and adaptive morphological operator. Two test images will be used to visualize the effect of all mentioned techniques. Therefore, Fig. 3.1 *lenna*, a popular test image, and Fig. 3.1 an *ultrasound image* were chosen. The ultrasound image was selected since its filtering is quite challenging due to presence of multiplicative noise. This may bear some similarities with the THz noise. In addition, the fuzzy set theory, which is exploited in some of these techniques, and a clustering method will be explained. For further visual clarification , their results on the sample images will be displayed.

Figure 3.1: Original images, left: lenna image, right: prostate ultrasound scan

3.2 Fuzzy Image Processing

There are many soft computing techniques available in literature for image processing. Nevertheless, in this thesis fuzzy set theory was used to design new techniques. Fuzzy techniques can simply use linguistic rules according to the domain knowledge about specific images. However, other soft computing techniques such as neural networks need many training data to be effective. In this case there are not that many data available to train the system. It would be very cost inefficient to capture many images with the current technology (slow image acquisition rate). Therefore, fuzzy logic seemed to be a very suitable technique for

processing of THz images. Since fuzzy set theory has been employed in several parts in this work, it is important to provide some information on this theory.

Fuzzy set theory was introduced by Prof. L. A. Zadeh of University of Berkeley in 1965 for representing approximate linguistic knowledge that cannot be explained by conventional (crisp) set theory [34] [35] [36] [37]. In conventional methods, truth is a bivalent category represented as 1 (true) and 0 (false). However, fuzzy set theory has introduced the idea of partial truth.

A fuzzy set is represented by *membership* functions, therefore an element in this set will have a degree of membership μ in that particular set. For example, a set of gray levels that share the property of darkness in an image can be defined with fuzzy set theory. To define this set, two thresholds are set (i.e. gray levels 50 and 150). All the elements between 50 and 150 have a partial membership in this set. However, all the gray level less than 50 are full members of the set, and all the ones higher than 150 are not the member of this set [38]. If classical set were used, one hard threshold would have been used (i.e. 100). Everything below that number is an element of the set, and anything higher is not a member. Fig. 3.2 illustrates this example.

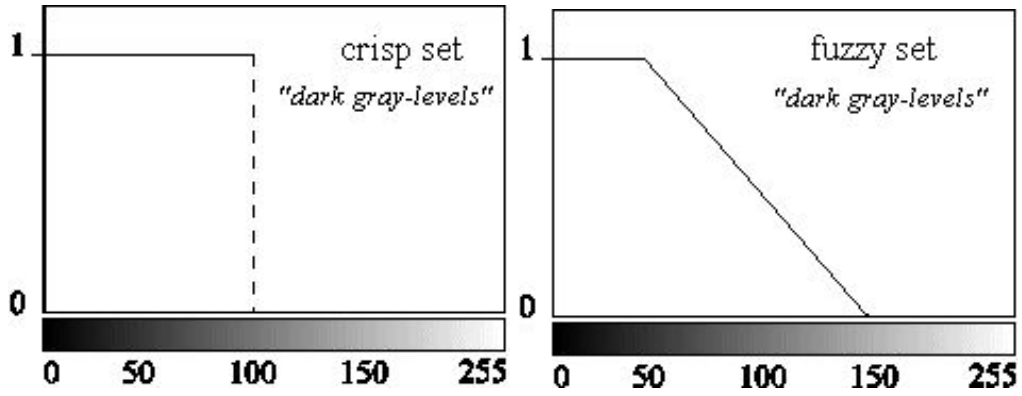

Figure 3.2: Illustration of the set "dark gray-levels". Left: a conventional two-valued (crisp) set, right: a fuzzy subset [source: [38]]

Fuzzy image processing has three main stages [38]: image fuzzification, modification of membership values, and, if necessary, image defuzzification (see Fig. 3.3).

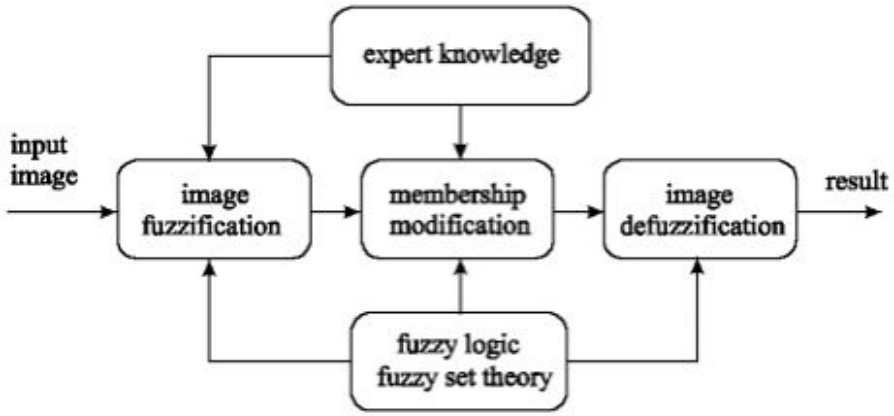

Figure 3.3: The general structure of fuzzy image processing [source: [38]]

In the case of image processing, fuzzification (Fig. 3.3) is the encoding of image data, and decoding of the results is the defuzzification (Fig. 3.3). The strength of fuzzy image processing is in the middle step, which is the modification of the membership values, Fig. 3.3 [38]. The modification of membership values is heavily influenced by the expert knowledge. After evaluating the expert views, appropriate fuzzy techniques are applied to manipulate the membership values. The techniques could be fuzzy clustering, a fuzzy ruled based approach, or a fuzzy integration approach [38].

3.3 Image Filtering

Not many works have been reported on filtering of THz images. In this work, the following filters were implemented to verify their effects. For sake of simplicity, the two test images are used first to observe the filtering effect.

3.3.1 Sticks Filter

To obtain better results for segmentation, pre-processing techniques are required as it was mentioned. After an extensive research, a very strong edge preserving filter known as "sticks" [40] was selected as one of the main filtering methods for this thesis. This filter is well

known in literature for its capabilities in detection of boundaries and lines in presence of multiplicative noise [41]. In this case, to find the defected region in materials with a high accuracy, it is crucial to conserve all boundaries.

To find the lines in the image, it is necessary to determine whether a line passes through each pixel. In sticks filter, a neighbourhood around each pixel is constructed and a search for lines passing through the center of that neighbourhood is performed. "This is an M-array hypothesis testing, where each of the hypotheses represents a possible line orientation" [40]. For simplicity, the neighborhood can be considered to have a square shape. This way, the number of orientations is equal to the number of hypothesis. The set of hypotheses is called "sticks". Fig. 3.4 shows a set of sticks of length 5 [41].

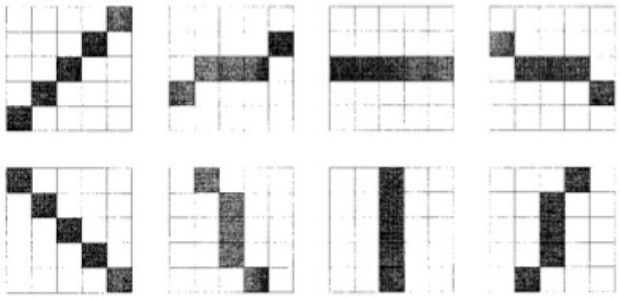

Figure 3.4: Stick orientations of length 5 [Source: [40]]

Generally, five different types of noise detection strategies can be followed [40]:

- Optimal detection
- Quadratic detection
- Generalized likelihood ratio detection
- Linear detection
- Rotating kernel transformations

In this thesis, optimal detection is used. This method in a maximum likelihood sense indicates that the target is presented within the signal or it is just noise. This is done by selecting a hypothesis which maximizes the likelihood ratio function [40]:

$$\Lambda_i(x) = \frac{P[x|H_i]}{P[x|H_0]}, \tag{3.1}$$

where x is the set of points in the neighbourhood, and H_i is the i-th hypothesis that passes through the center of the neighbourhood, and H_0 is the null hypothesis. The ratio is the likelihood of the target present in the signal over the likelihood when no target is present.

In addition, optimal selection of the length and width of the sticks is essential. It is a tradeoff between line enhancement and noise reduction. Longer sticks achieve better line enhancement with less noise reduction. However wider sticks are more sensitive to noise with dimmer boundaries. In chapter 4 both wider and thinner stick are tested on THz images. In this section to show the effect of this filter, a 21 pixels in length and one pixel in width stick was chosen to apply on both *lenna*, and the *utrasound* images. Fig. 3.5 shows the result on the sample images.

3.3.2 Frost Filter

Frost filter is known as one of the "edge preserving" filters [42] and is well known for its ability to reduce speckle noise. In this thesis, the Frost filter is applied on THz image for noise reduction in some of the samples in the Chapter 4. Frost filter "uses an exponentially damped convolution kernel that adapts to regions containing edges by exploiting local statistics" [42]. The output is evaluated as follows:

$$I = \sum_{p \epsilon \eta} m_p I_p, \tag{3.2}$$

where [42],

$$m_p = exp(-KC_s^2 d_{s,p}) / \sum_{p \epsilon \eta_s} exp(-KC_s^2 d_{s,p}), \tag{3.3}$$

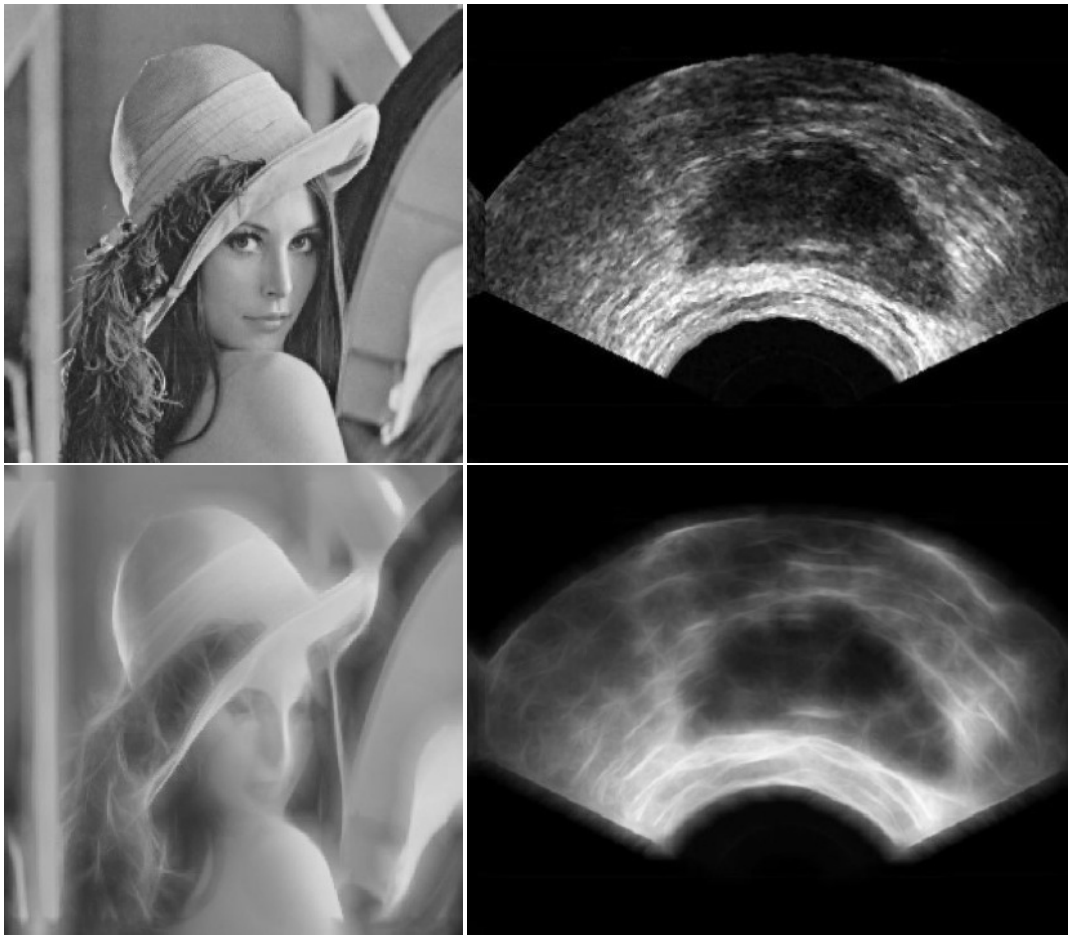

Figure 3.5: The effect of sticks filter, l= 21 and w=1

$$d_{s,p} = \sqrt{(i - j_p)^2 + (j - j_p)^2}. \tag{3.4}$$

Here, η_s is the filter window, K is the damping factor, (i, j) are the grid coordinates of pixel s, and (i_p, j_p) are coordinates of pixel p.

The outcome of this filter is shown in Fig. 3.6. This filter was not very strong in comparison with the sticks filter on the examined samples. However, the combination of this filter with other filters, which is shown in Chapter 4 was satisfactory.

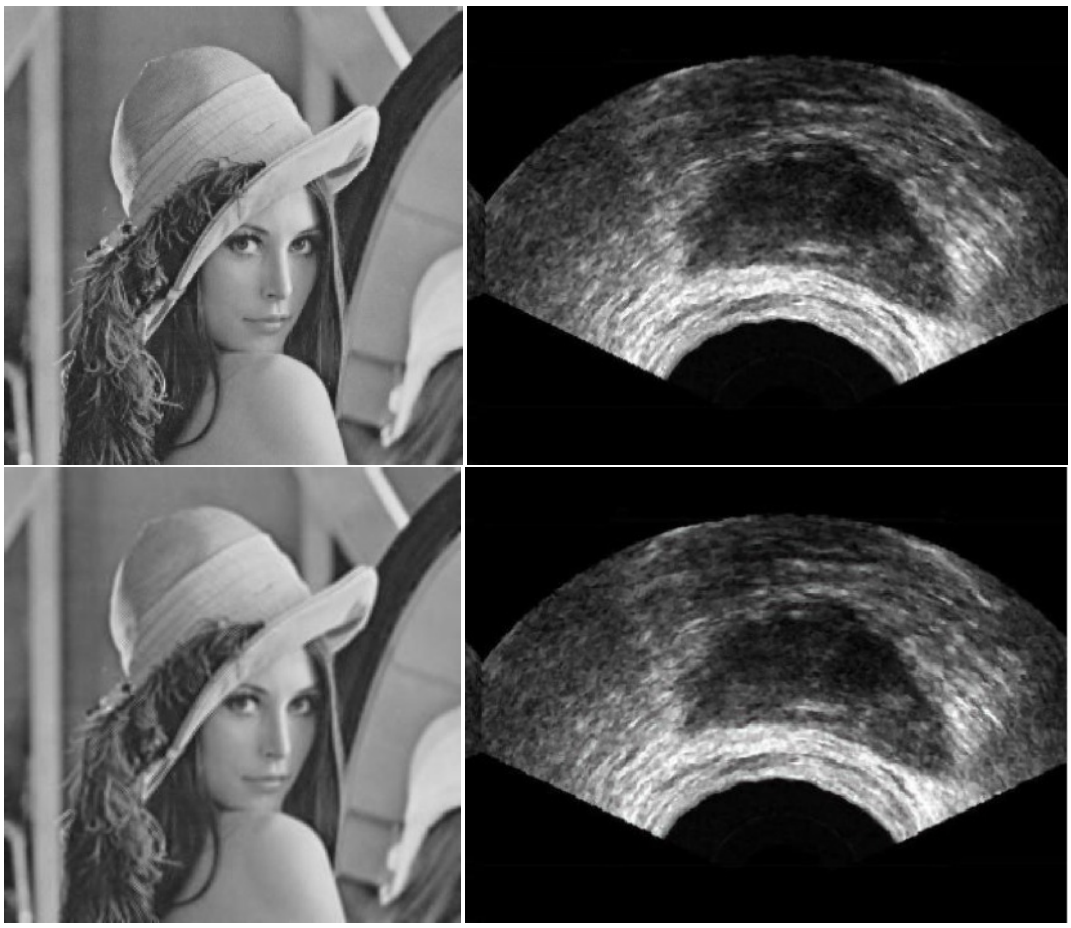

Figure 3.6: The effect of Frost filter, η_s=1 and K=1

3.3.3 Wiener Filter

Wiener filter has been one of the most-established filters in image processing. This filter was introduced by Norbert Wiener in 1949 [43] and is ideal for normally distributed noise. This is an optimal estimator in the sense of minimizing mean squared error (MSE) for stationary Gaussian processes [44].

This filter works as follows:

$$Y = X + N, \tag{3.5}$$

where, Y is the noisy image, X is the noise-free image, and N is the additive Gaussian noise. The goal is to remove the noise from image and find a linear estimator $\hat{X}$ of X, which minimizes the mean square error (MSE) [44],

$$MSE = 1/n \sum^{n} (\hat{X} - X)^2, \tag{3.6}$$

where n is the number of elements.

By using Wiener filter, the majority of the additive white Gaussian noise can be removed. However, THz images have possibly other sources of noise. Therefore, in this thesis a fuzzy fusion of Wiener and Median filter was implemented to use the strength of both filters for noise removal. To demonstrate the impact of this filter a Wiener filter in 5×5 neighbourhoods was applied on the test images in Fig. 3.7.

3.3.4 Median Filter

Another well-established filter in literature is the median filter. This edge preserving filter is a non-linear filtering technique and is optimal for removing impulsive noise [45], also called outliers. Median filter replaces the central value of an $M \times N$ neighbourhood with the median value of all the points within that neighbourhood. This is done by sorting the values in that neighbourhood to find the median value. In this thesis, to combine the benefits of two filters, the median filter was fused with Wiener filter. The results on THz images will be shown in Chapter 4. The filtering effect for test images can be observed in Fig. 3.8.

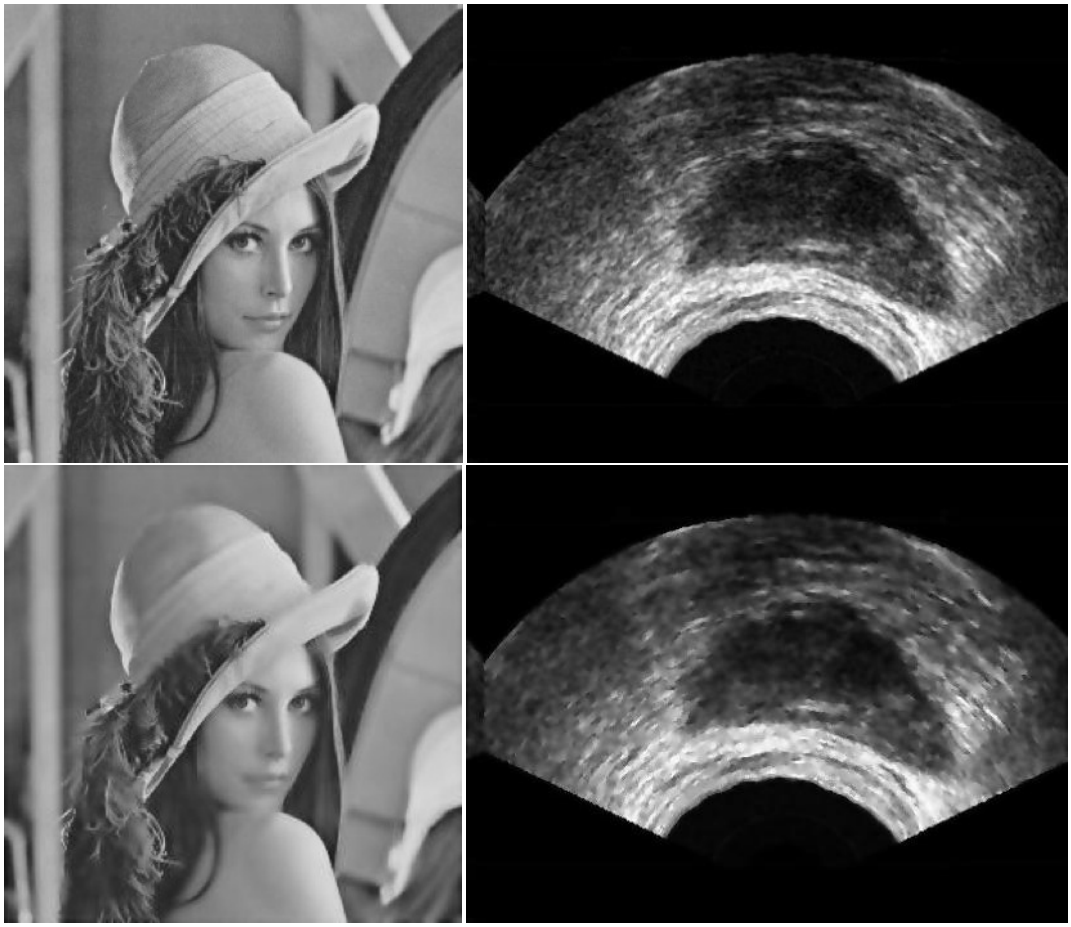

Figure 3.7: The effect of Wiener filter in 5×5 neighbourhoods

3.4 Contrast Adjustment

Histogram-based and morphological methods have been investigated to further increase the image quality beyond the noise removal.

3.4.1 Adaptive Histogram Equalization

Histogram Equalization is a common method for modifying the contrast of an image. It equalizes the gray-level distribution in such a way that the intensity histogram has a desired shape, generally a uniform distribution. Histogram equalization employs non-linear and non-monotonic transfer functions. This method maps the intensity values of pixels in the input

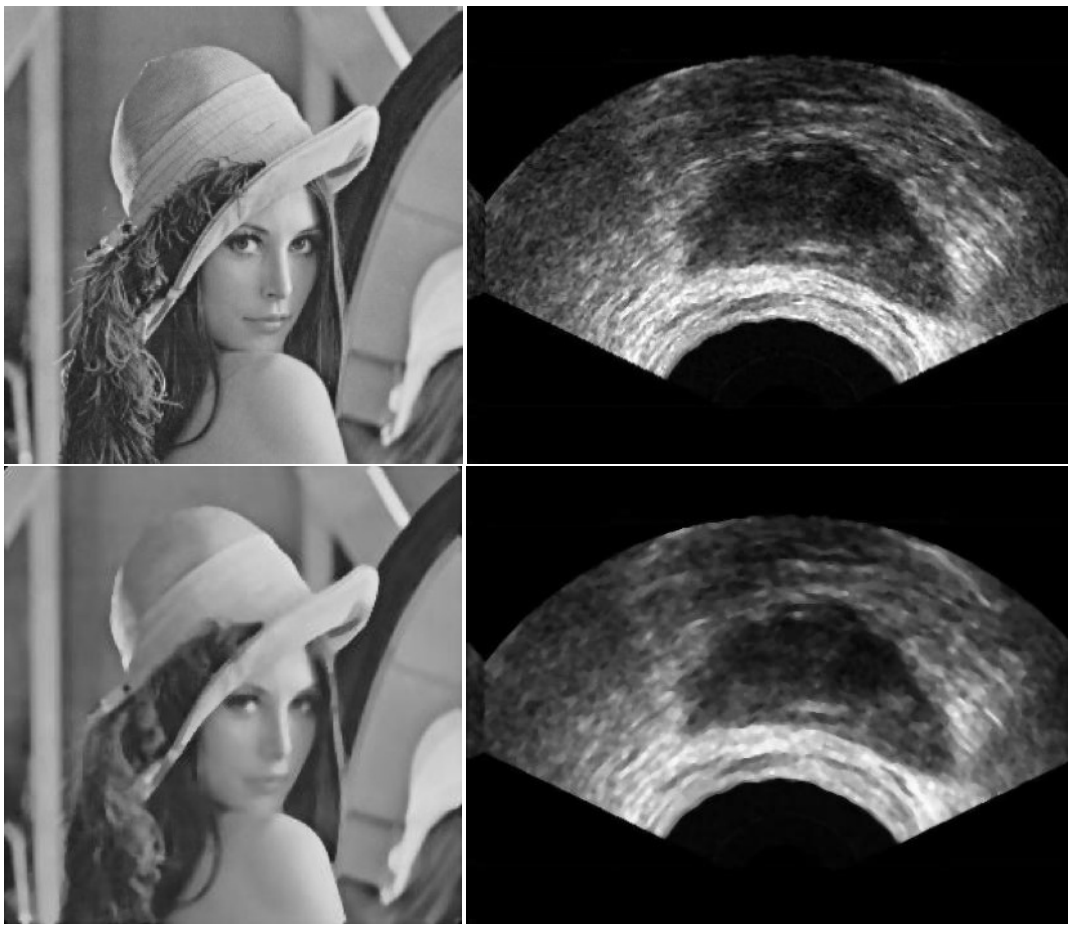

Figure 3.8: The effect of median filter in 5×5 neighbourhoods

image such that the output image contains a uniform distribution of intensities [48]. In this work, an adaptive equalization method has been employed, which works on small regions instead of processing the entire image. Each regions contrast is enhanced individually in such a way that the histogram of the output region approximately matches the desired histogram. The neighbouring regions are combined by bilinear interpolation after processing the whole image region by region. This avoids artificially induced boundaries, the so-called chess-board effect. Fig. 3.9 shows the result after using the adaptive histogram equalization applied on the test images.

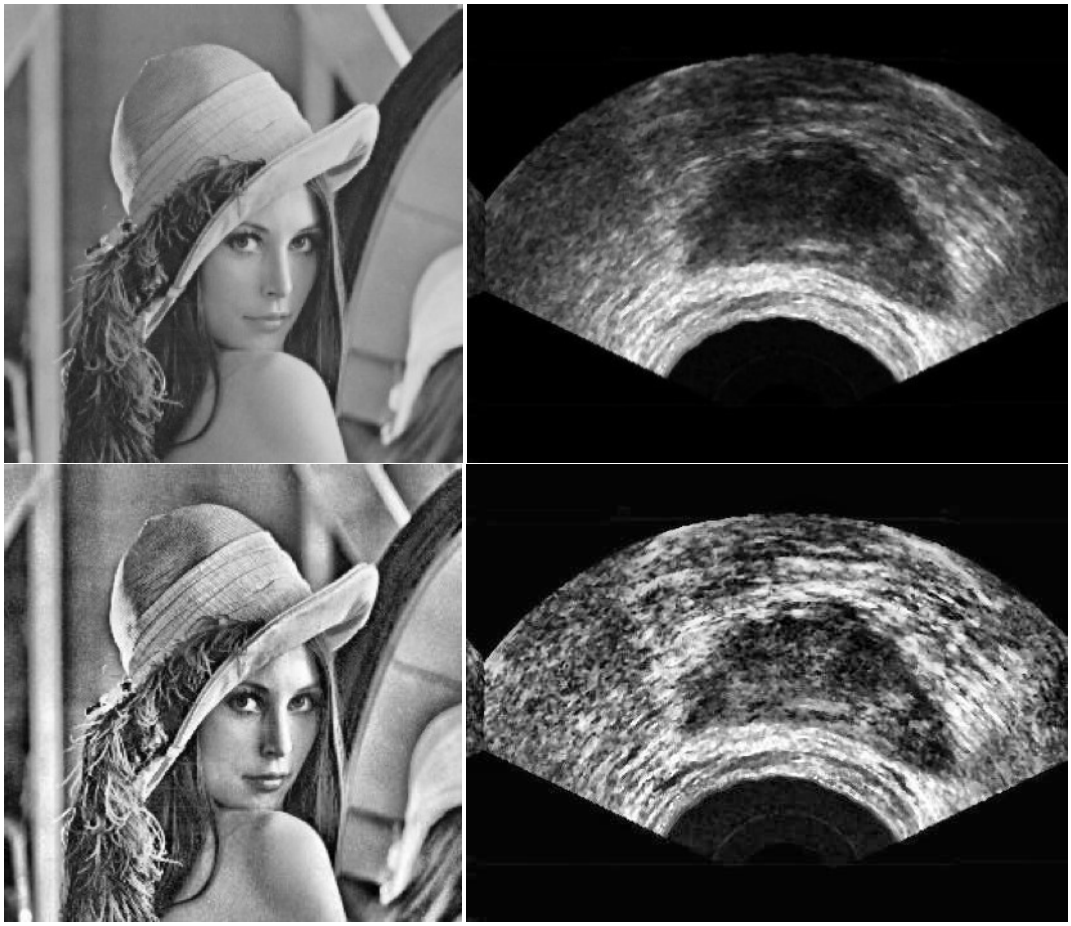

Figure 3.9: The effect of Adaptive Histogram Equalization in 8×8 regions

3.4.2 Adaptive Morphological Operator

Morphological operations such as erosion and dilation are generally used to filter an image and change the brightness distribution [46]. However, it is not always possible to determine which method, erosion or dilation, is the most appropriate techniques. This also applies to extended morphological operations such as opening and closing. Fuzzy techniques [38], [39] are suitable methods to gradually or partially switch between different methods. If erosion of an 3×3 neighborhood is noted by $E^{+1}_{n=-1} I(i+n, j+n)$, where $I(i,j)$ is the intensity of the image at the location (i,j), and the dilation is noted by $D^{+1}_{n=-1} I(i,j)$, then the new gray-level $I^{'}(i,j)$ can be calculated as follows:

$$I^{'}(i,j) = \mu_{dark}(i,j) \times E^{+1}_{n=-1} I(i+n, j+n) + (1 - \mu_{dark}(i,j)) \times D^{+1}_{n=-1} I(i,j), \tag{3.7}$$

The membership function $\mu_{dark}(i,j)$ for darkness can be calculated based on a sigmoidal function:

$$\mu_{dark}(i,j) = 1 - \frac{1}{1 - \exp I(i,j)}. \tag{3.8}$$

The effect of the fuzzy-controlled morphological operation for the test images is illustrated in Fig. 3.10.

3.5 Image Segmentation

Clustering methods are very common for image segmentation. A group of pixels which are similar in terms of their gray levels are clustered together. After clustering, the image can be re-grouped in different gray level groups, or simply in black and white (binary). There are numerous techniques available for this purpose. In this thesis, a very common clustering method, K-means, is compared to the developed local adaptive Otsu thresholding method. The Otsu method is also a very popular method in literature. In chapter 4 a locally adaptive version of this established method has been developed to segment the images in $M \times N$ sub-images.

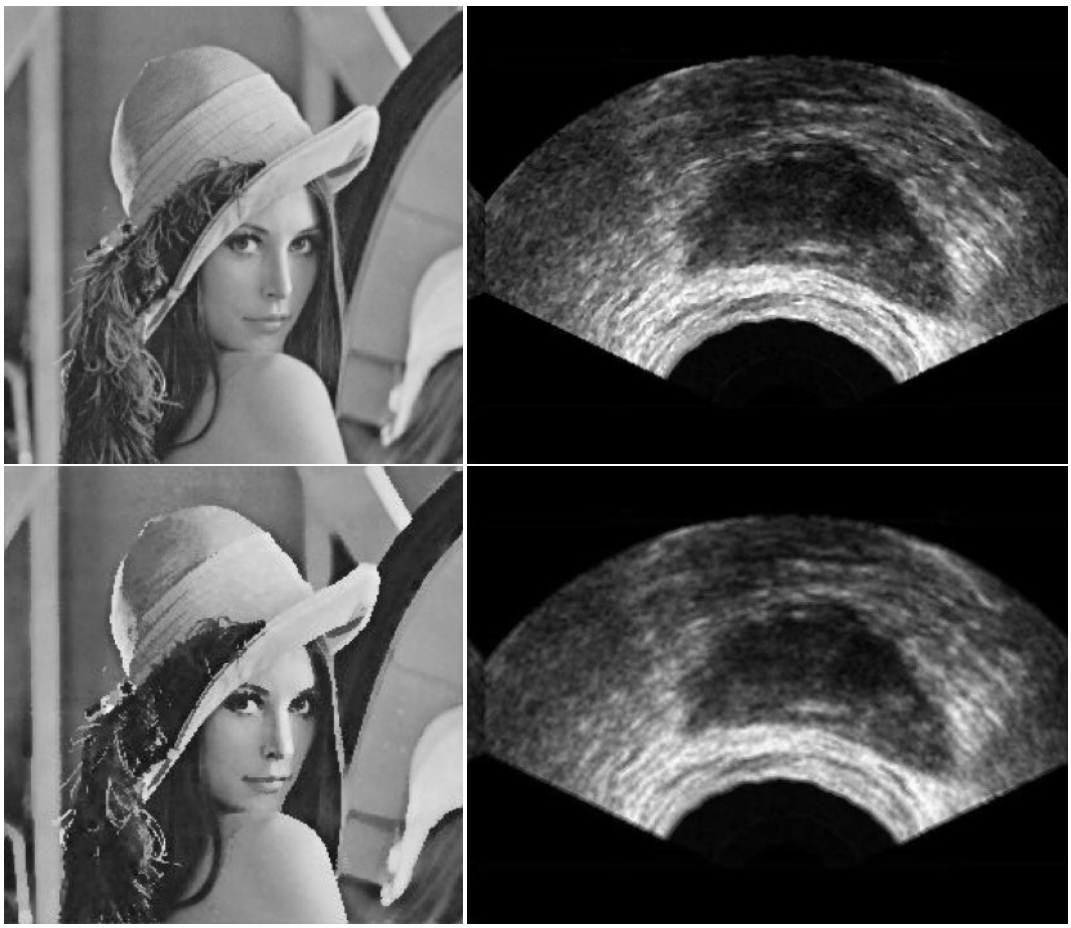

Figure 3.10: The effect of Adaptive Morphological Operator in 8×8 regions

3.5.1 K-Means Clustering

The main goal of K-means clustering is to divide the data into k clusters such that the relative distance to the centroids of each cluster is minimized for all data. In other words, an objective function needs to be optimized [49]:

$$J = \sum_{j=1}^{k} \sum_{i=1}^{n} ||x_i^{(j)} - c_j||^2, \tag{3.9}$$

where x is the data point and c is the class centroid.

K-means algorithm starts by partitioning the input points into k initial sets. It then calculates the mean point, or centroid, of each set. It constructs a new partition by associating each point with the closest centroid. Then the centroids are recalculated for the new clusters, and algorithm is repeated by alternate application of these two steps until convergence, which is obtained when the points no longer switch clusters [49].

K-means algorithm could be applied with two different procedures:

- Assign each object to a cluster
- Set initial positions for the cluster centroid

The first procedure is as follows:

- The position of the k centroids are determined
- An optimization method is then used to re-assign some of the objects to different clusters by using the previous objective function
- New centroids are determined
- This procedure is continued until the optimal objects cluster assignment is found.
- The objects are randomly assigned to one of the k clusters

The second procedure is as follows:

- Place k points into the space represented by the objects that are being clustered. These points represent initial group centroids.
- Assign each object to the group that has the closest centroid.
- When all objects have been assigned, recalculate the positions of the K centroids.
- Repeat Steps 2 and 3 until the centroids no longer move

By applying either of these two procedures the image can be segmented into several segments. complete illustration of this method can be found in Chapter 4.

3.5.2 Summary

As it was discussed, THz images are difficult to segment since the noise type is not recognized in literature. Also, THz images have low signal to noise ratio. Several techniques have been proposed in this chapter for filtering and segmentation of these images. Filters such as sticks, Frost, median, and wiener. In addition, clustering methods such as K-means have been investigated. However, in this preliminary work in THz imaging various other methods have been developed to improve and segment THz images.

Chapter 4

Proposed Algorithms and Results

The goal of this thesis is segmentation of THz images through different image processing techniques to locate possible manufacturing defects. All these methods are considered to be image-based and are not based on the optical properties of the samples. The advantage of these processes is that very little information about the sample is required. For instance, it is not easy to evaluate the complex refractive index [1], if the depth of the samples are not known, or the samples are not consistent. Image processing techniques generally are designed on the assumption that similar pixels are likely to have similar properties and, hence, can be processed in the same way.

To be able to segment THz images, several techniques were introduced in chapter 3. In this chapter all those methods plus proposed methods are applied to THz images, and their results are displayed through visual and analytical representations. There are two main samples that were tested in this chapter. First, composite materials which are used in aerospace industry were examined for defect detection. Second, a phantom sample (containing circles of different sizes) was crafted to conduct general accuracy measurements.

4.1 Defect Detection in Composite Materials

For the first time, composite materials that are used in the aerospace industry (provided by Pratt & Whitney Canada), were under examination with THz cameras. Due to novelty of this process, selection of the ideal frequency for defect detection was challenging. After extensive research and investigating diverse frequency ranges in both transition mode and reflection mode, the ideal frequency was localized[1].

After capturing the images, the proposed solution was put in to the effect. To improve the SNR, sticks filter [40] was applied to the THz Images. This filter is a very powerful tool to enhance the boundaries in any type of imaging with a low SNR, and high speckle noise. It is common in literature to use this type of filter for ultrasound images [40]. In this thesis, this filter was used on Terahertz images. After observing the result from sticks filter, a fuzzy technique was developed to fuse the phase and amplitude images. The amplitude image is generally brighter than the phase image, and the object of interest appears bright. In contrast, the phase image is darker than the amplitude image, and the object of interest appears dark. However, the discrimination is quite vague and not distinct enough. This motivates us to use fuzzy rule-based approach to exploit this characteristic in order to detect the defected part by fusing information from both THz images.

In this work, there are two different samples under testing. The first one did not contain any defect. However, the second sample contained a defect which was purposefully applied in a shape of a rectangle. The imaging device is mounted in a gantry stage, which took the images by raster scan.

Two imaging geometries are possible with this system: collinear and small angle (pitch-catch). Both of them are reflection geometries. The polarization of the radiation in the collinear reflection is circular and linear in the pitch-catch geometry. The raw output of the system is in log scale. The data is converted to linear scale as follows:

$$y = 10^{\frac{-20.289x^2+84.194x-93.836}{20}}. \tag{4.1}$$

[1]Due to confidentially agreements with our industrial partner, these frequencies can not be disclosed.

Fig. 4.1 displays how the sample is moving in the desired (x,y) direction for complete scanning of the probe.

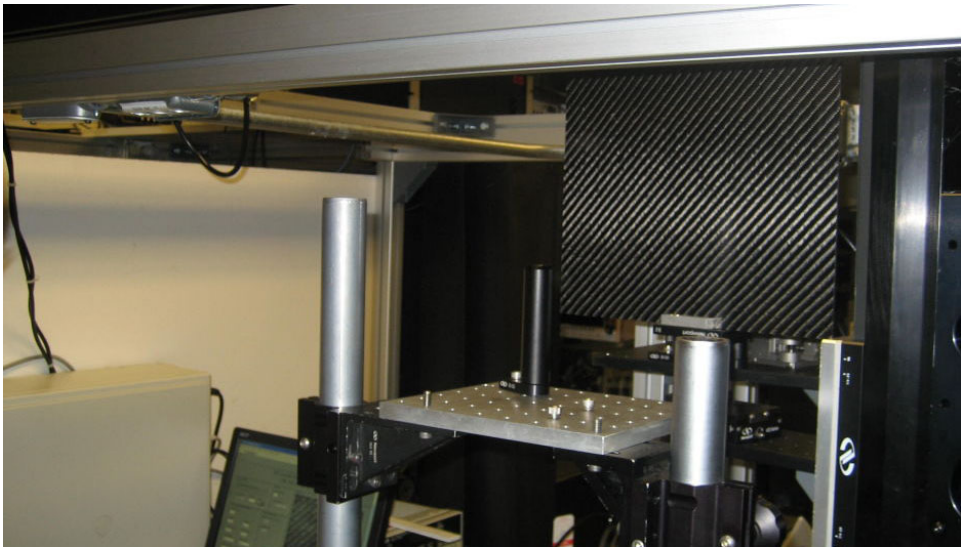

Figure 4.1: Process of scanning the composite material

Sample images taken can be seen in Fig. 4.2 (with no defect) and Fig. 4.3 (with defect).

To validate the proposed solution, the algorithm was applied on the images that were captured by the CW THz machine. First, sticks filter was applied. For the phase image, a 21 pixels in length and one pixel in width stick was depicted, in 8 different directions. For the amplitude image, a 21 pixels in length and three pixels in width stick was chosen in 8 different directions.

As it was mentioned in chapter 3, longer sticks achieve better line enhancement with less noise reduction. However, wider sticks are more sensitive to noise with dimmer boundaries. The amplitude image contains more noise than the phase image. Therefore, wider sticks were chosen for these images. By looking at Fig. 4.4, and Fig. 4.5, one can observe a significant difference in both amplitude and phase images of the original images and the sticks-filtered images.

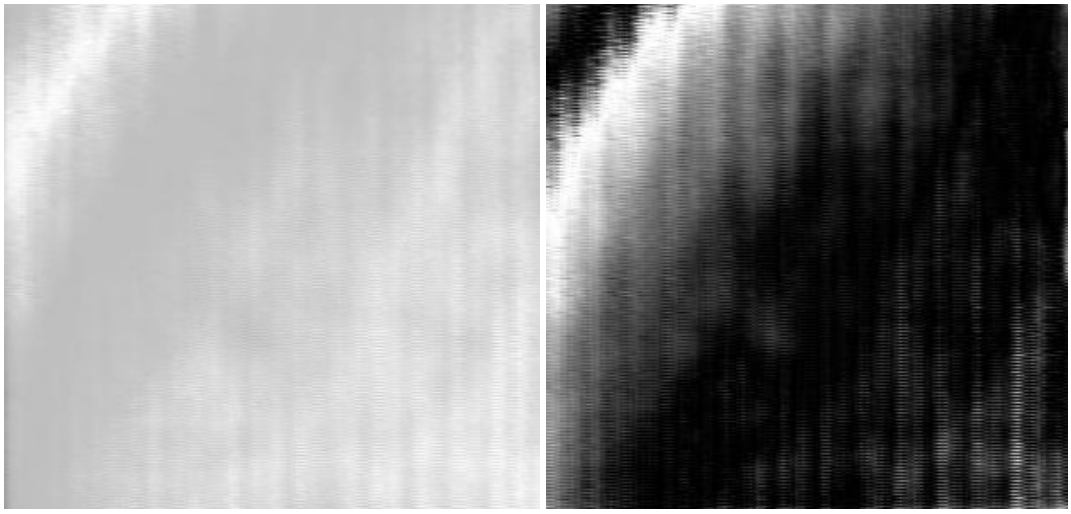

Figure 4.2: Amplitude and phase image of sample 1

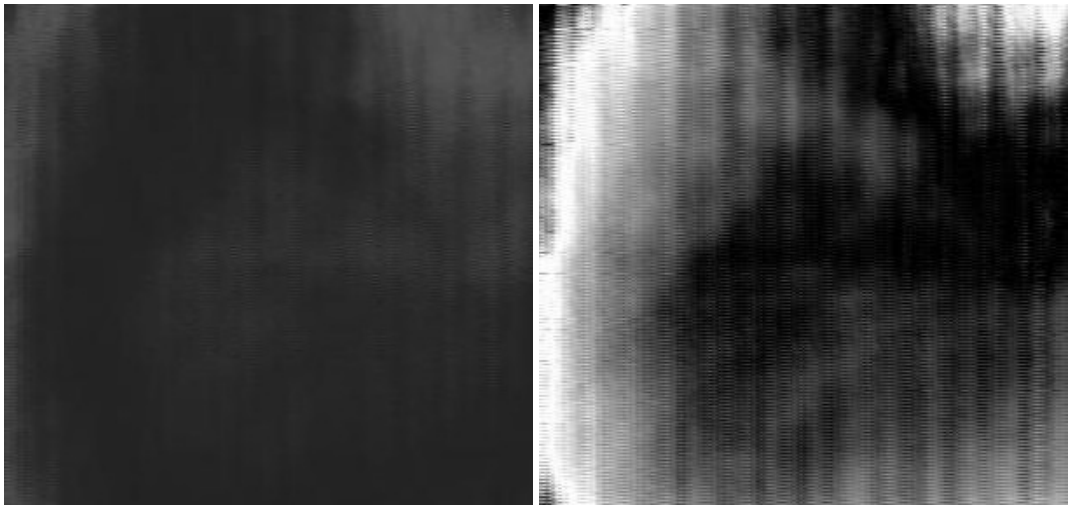

Figure 4.3: Amplitude and phase image of sample 2

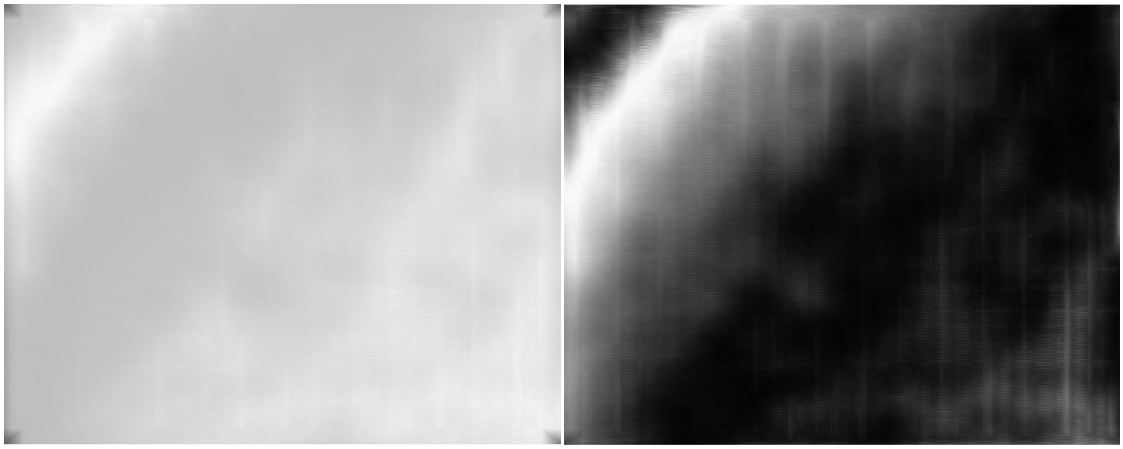

Figure 4.4: Stick filtering of amplitude and phase image of sample 1

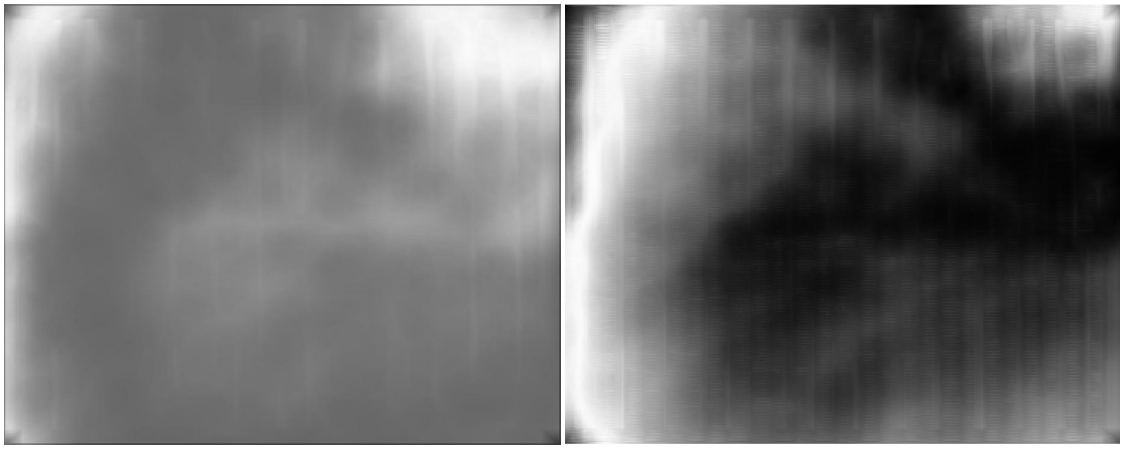

Figure 4.5: Stick filtering of amplitude and phase image of sample 2

4.1.1 Fusion of Phase and Amplitude Images

In this thesis, a simple fuzzy technique is proposed to fuse the phase and amplitude images. This soft computing method was used because one can simply define rules according to the domain knowledge. A rule-based fusion seems to not only be easy for implementation but also effective for segmentation.

By fusing the amplitude and phase images, the crucial information (i.e. defect) from both images can be obtained. The gray scale of the amplitude images are determined by the peak to peak amplitude of the waves at each pixel. In addition, phase images are formed

using the arrival time of the THz waves. Amplitude images are brighter in nature and phase images are darker. Besides the appearance of defects in amplitude and phase images are widely distinct. However, the noisy and imprecise data cannot easily be segmented.

The fusion algorithm processes the filtered images in $2w+1$ neighborhoods. In the phase image, the membership of brightness is calculated in each neighborhood using a standard S-function. The median value of the neighborhood is calculated to determine its brightness. In the amplitude image, the membership of darkness is calculated in each neighborhood using a standard Z-function. The median value of the neighborhood is determined to determine its darkness. Only one rule is used to fuse the phase and amplitude image:

IF the neighborhood is *dark* in the phase image
AND the neighborhood is *bright* in the amplitude image,
THEN make that pixel *bright* in the result image.

The pseudo code for the fusion is given in Table 4.1.

In Fig. 4.6, the fusion of phase and amplitude for both samples are displayed. The result of segmentation can be seen in Fig. 4.7.

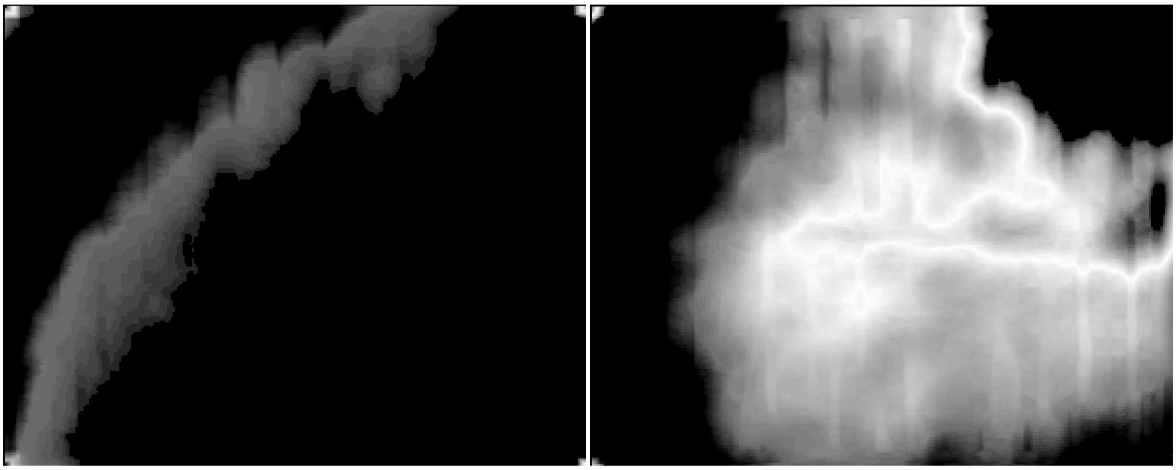

Figure 4.6: From left to right: fusion for sample 1 and 2

By observing the null segmentation in Fig. 4.7, it is apparent that there are not any defects in the sample 1. However, the defected region was segmented in sample 2. This

Table 4.1: Fusion Algorithm

Determine the number of rows R and columns C of images

Set the window step $w \in \{1, 2, 3, \dots\}$

Set a_P, b_P for the S-function: $\mu_P(a_P) = 0, \mu_P(b_P) = 1$

Set a_A, b_A for the Z-function: $\mu_P(a_P) = 1, \mu_P(b_P) = 0$

Set the number of output intensities L

for i=w:R-w

  for j=w:C-w

    Calculate the typical value in the phase image P

      $\tau_P = \text{median}_{k=1\dots w} P(i-k : i+k, j-k : j+k)$

    Calculate the typical value in the amplitude image A

      $\tau_A = \text{median}_{k=1\dots w} A(i-k : i+k, j-k : j+k)$

    Calculate the membership *dark* in the phase image

      $\mu_P^{bright}(\tau_P) = S(\tau_P; a_P, b_P)$

    Calculate the membership *bright* in the amplitude image

      $\mu_A^{dark}(\tau_A) = Z(\tau_A; a_A, b_A)$

    Calculate the intensity in the output image

      $F(i,j) = \min(\mu_P^{bright}, \mu_A^{dark}) \times (L-1)$

  end

end

Figure 4.7: From left to right: Null segmentation for sample 1 (no defect), segmented defect for sample 2

defect which was in a rectangular shape is shown in Fig. 4.7. This result is very promising due to novelty of the THz imaging technology. However, for a larger number of test images, "no defect" may not necessarily results in a "null segmentation". We did not encounter this case. Nonetheless, if this occurs, then additional validation techniques are required to distinguish between "defect" and "no-defect" cases.

The overall results for defect detection can be summarized as follows:

1. From six samples, three were defected and three had no defects
2. THz waves could only penetrate through composite material in a very narrow window of frequencies
3. Even for located penetrating frequencies, the penetration depth was limited
4. Only one out of three defected samples could be classified as such (see Fig. 4.7)
5. The defects were purposefully implanted inside the samples and had certain shapes and dimensions, however, for the detected defect it was apparent that the exact shape of the defect has not been correctly captured

6. Image acquisition via THz radiation is still a time consuming process, resulting in a limited number of images for this investigation

7. Most likely it is too early to make any general statement, however, it seems that the located THz frequencies are rather specific than sensitive with respect to defect detection in composite materials

In order to find out the spatial limitations of THz imaging and due to the fact that working with the composite images was rather cumbersome, we designed and carried out second series of investigation using a phantom object. The results are reported in the following section.

4.2 Accuracy Measurements via Phantom Samples

Due to several limitations, capturing a large number of test images was not possible. Hence, to provide accuracy measurements for THz imaging, a phantom was built. This phantom, Fig. 4.8, contains circles with different sizes. There are 41 circles, and the range of their radii are from 0.06 inch up to 1 inch. This way the accuracy can be measured with wide range of samples. This phantom was placed under the CW THz machine for imaging at Rensselaer Polytechnic Institute. Fig. 4.9, displays how the phantom is moving in the desired (x,y) direction for complete scanning of the sample. The image taken can be seen in Fig. 4.10. The images were taken at 1.63 THz, which has the highest output power of 181 mW for this particular system. Better resolution can be observed with higher output power. Fig. 2.8 shows all different frequencies that are available at RPI for this particular continuous-wave THZ system.

To be able to segment the Fig. 4.10, different filtering methods were applied before the segmentation methods. Filtering should improve the SNR, and consequently edge detection should be much easier. In this section many different filtering and image processing techniques were applied to the sample. These methods are Frost filter, Frost filter plus ultra filter (see next paragraph), sticks Filter, adaptive histogram equalization, and adaptive morphological operator.

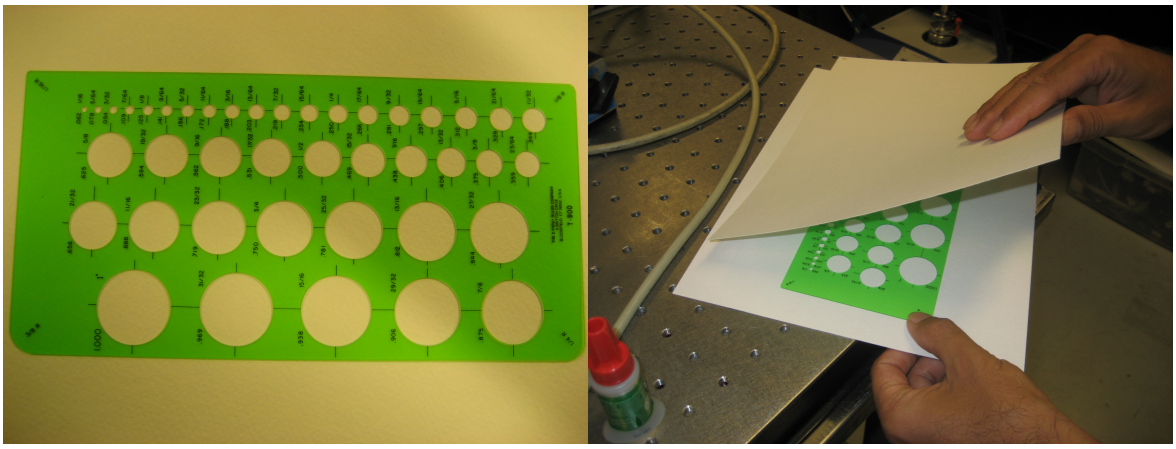

Figure 4.8: Building a phantom. Left: the real sizes of the circles, right: process of making the phantom

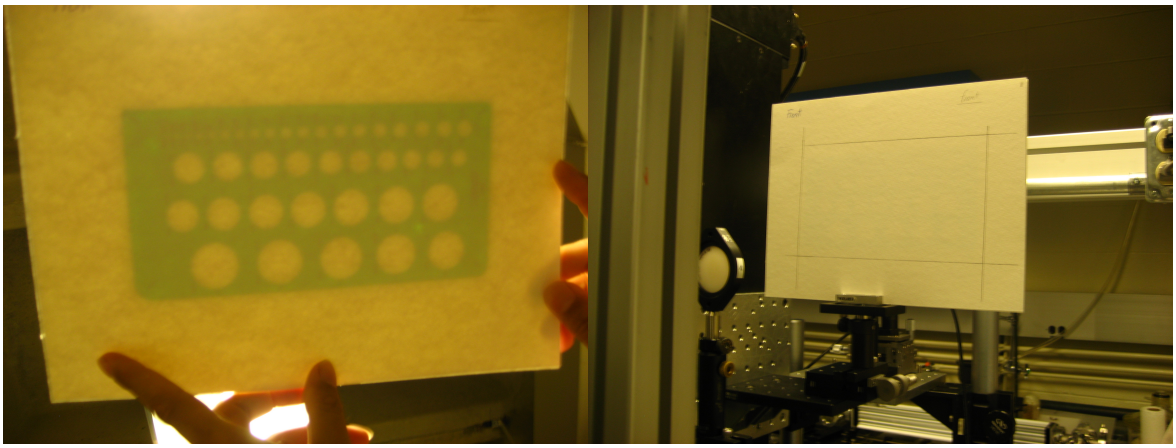

Figure 4.9: Phantom sampling. Left: The phantom is shown under the bright light, right: capturing phantom images by using the THz gas laser

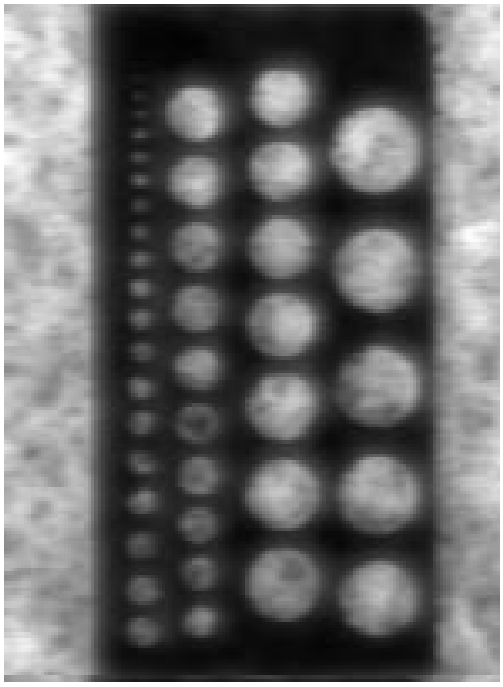

Figure 4.10: The THz Phantom

There are many established techniques that can be applied to remove the noise. Median and Wiener [43] are arguably the most popular methods. In this thesis, both filters are fused to be able to combine their respective strengths in removing different noise types. Before these two well-known filters, the Frost filter [42] was used to reduce speckle noise. After filtering the images, a new contrast adjustment technique is applied to Terahertz images to enhance their brightness distribution. The combination of this method with fusion of Wiener and Median filters is called the *ultra filter*. The rest of the methods were explained in chapter 3.

After pre-processing, the image is ready for segmentation. K-means clustering and Otsu algorithm were tested for phantom segmentation. However, global or histogram-based implementation of Otsu method did not provide satisfactory results. Therefore, a locally-adaptive Otsu thresholding was developed in this work.

4.2.1 Fusion of Median and Wiener

Median and Wiener [43] are among the popular filtering techniques in the field of image processing. These two classical filters will improve the SNR of the Terahertz images by removing impulsive and Gaussian noise, respectively. Even though Terahertz images are quite different from other modalities, Median and Wiener filters haven been used in literature to enhance Terahertz images as well. However, as it was mentioned before, scientists are not sure what type of noise Terahertz images possess. In this work, we fuse both filters to combine their strengths. To fuse these two filters, fuzzy techniques have been employed and proper membership functions have been defined to minimize the noise. In order to perform the filter fusion, the first step would be to determine whether a pixel is impulsive noise or not.

In equation 4.2 the likelihood of an pixel being outlier is calculated. In the mentioned equation, the center pixel g_{mn} is compared to all the surrounding pixels in a 3×3 neighborhood. The parameter w is the window size, and the tolerance $\Delta = 64$ was chosen heuristically:

$$P_{outlier} = min\left(1, \frac{\sum_j \sum_i |g_{ij} - g_{mn}|}{(w^2 - 1) * \Delta}\right), \tag{4.2}$$

If M and W represent the filtering results by Median and Wiener filters, respectively, then the fusion can be performed via a convex combination:

$$I^{'} = P_{outlier} \times M + (1 - P_{outlier}) \times W. \tag{4.3}$$

Hence, if a pixel is more likely to be an outlier, the result of the Median filter will be given a higher weight, otherwise the new pixel will be mainly determined through Wiener filtering. The result of the Frost filter and it's combination with the fusion of Median and Wiener can be seen in Fig. 4.11.

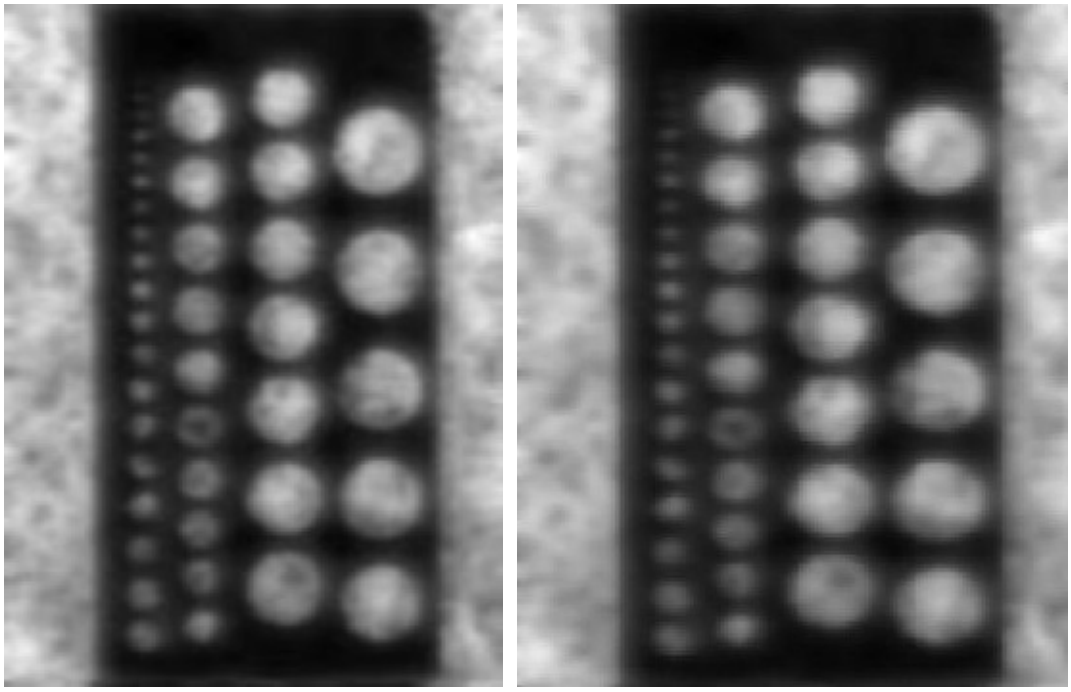

Figure 4.11: Phantom filtering. Left: The result of Frost filter, right: Frost filter plus fusion of Median and Wiener filters

4.2.2 Contrast Adjustment via Fuzzy Rules

To enhance the contrast of the Terahertz images, an adaptive contrast adjustment method was implemented. By doing this, the bright spots (the circles in the phantom image) can be segmented easier.

To adjust the contrast, first the neighborhood was captured by defining a step size $w/2$. Then, the typicality of the gray level in that neighbourhood was defined by taking the median of that neighborhood. Based on the grayness typicality, two membership functions were calculated, one for darkness μ_{dark} and one for brightness μ_{bright}. The modified gray levels g' are calculated as follows:

$$g' = \frac{\mu_{dark} \times S_1 + \mu_{bright} \times S_2}{\mu_{dark} + \mu_{bright}}, \tag{4.4}$$

where $S_1 = 1$ and $S_2 = 256$ are output singletons.

4.2.3 Frost & Ultra Filter

In this section Frost filter, which is known for speckle noise removal is combined with ultra filter for optimal noise reduction. The ultra filter is the fusion of Median and Wiener plus a contrast enhancement technique. After many trial and error combinations of different filters, this combination achieved exciting results. Fig.4.12 is the result of the Frost plus the ultra filter.

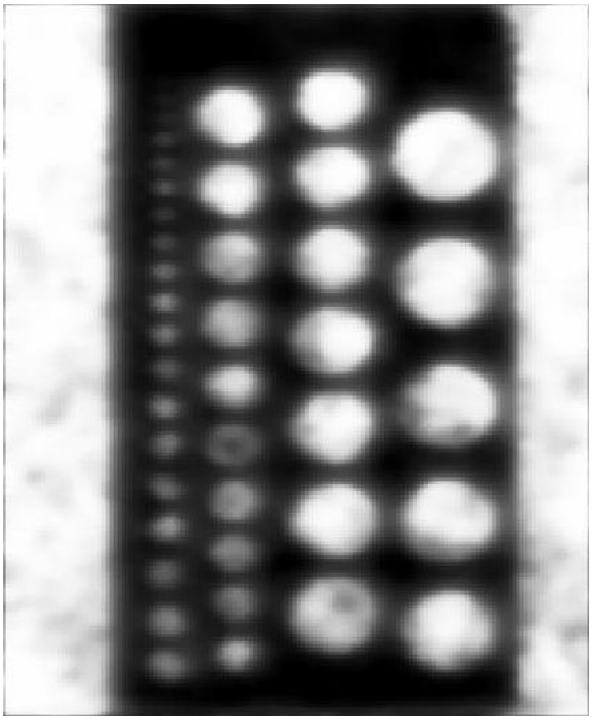

Figure 4.12: The result of Frost filter, followed by the designed Ultra filter junk

4.2.4 Sticks Filter

There are many ways to use sticks filter because of the property of switching the length and thickness sticks. In this thesis, 21 pixels long stick was applied on the extremely noisy composite material. The noise of the image in THz images depends on the material as it was discussed in 2.2.3. For the phantom material, which is cardboard and plastic, the amount of noise is significantly lower than composite materials. Therefore, shorter sticks were designed

to remove the noise. Two different sizes were chosen for comparison purposes. A 7 pixels in length and one pixel in width stick, and also a 5 pixels in length and 2 pixels in width were selected. Promising results were produced with this filter as shown in Fig. 4.13.

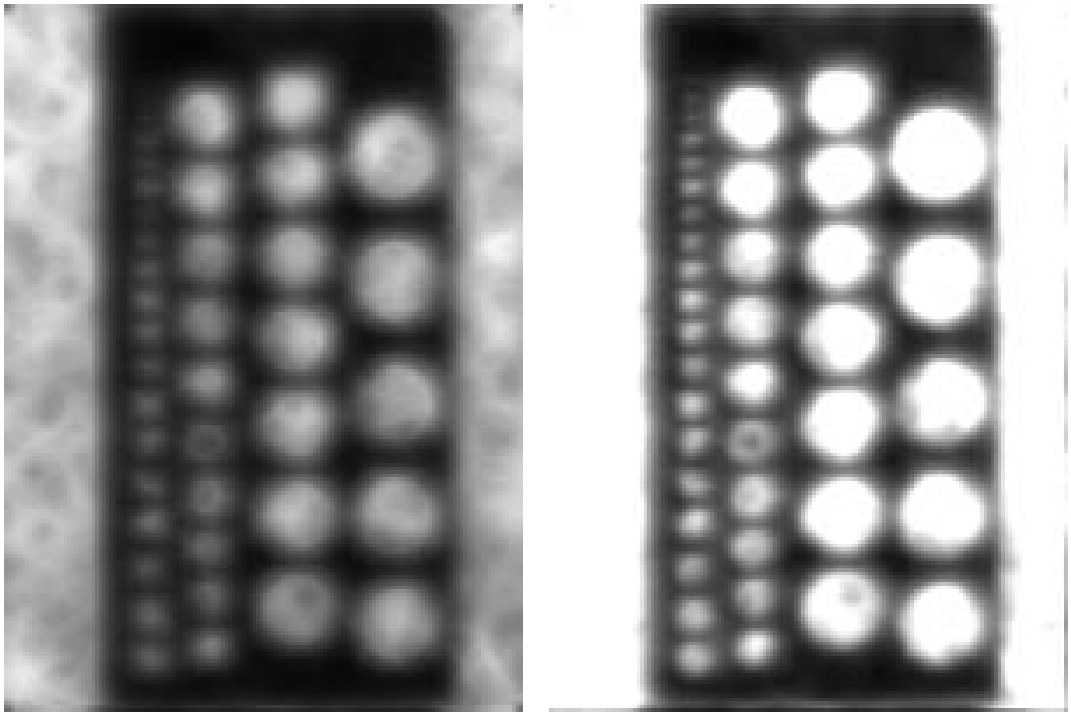

Figure 4.13: Stick filtering. Left: $l = 7, w = 1$, right: $l = 5, w = 2$

4.2.5 Adaptive Histogram Equalization

Adaptive histogram equalization is an enhancement method popular in both research and industry. It is based on the histogram of the image which is the occurrences of each intensity value in the image. Histogram equalization spreads out the most frequent intensity values to adjust the image contrast. As it was explained in chapter 3, adaptive histogram equalization operates in small neighborhoods/resgions and at the end combines all regions by using bilinear interpolation. For the conducted experiments, 8×8 neighborhoods were selected. This method was applied to the phantom image for comparison purposes. Fig. 4.14 demonstrates the results of adaptive histogram equalization. Also, the result of ultra

filter after this method is displayed. This step provides us with the information that Frost filter, which is used for speckle noise has improved the images significantly, and it is a more satisfactory combination with the ultra filter.

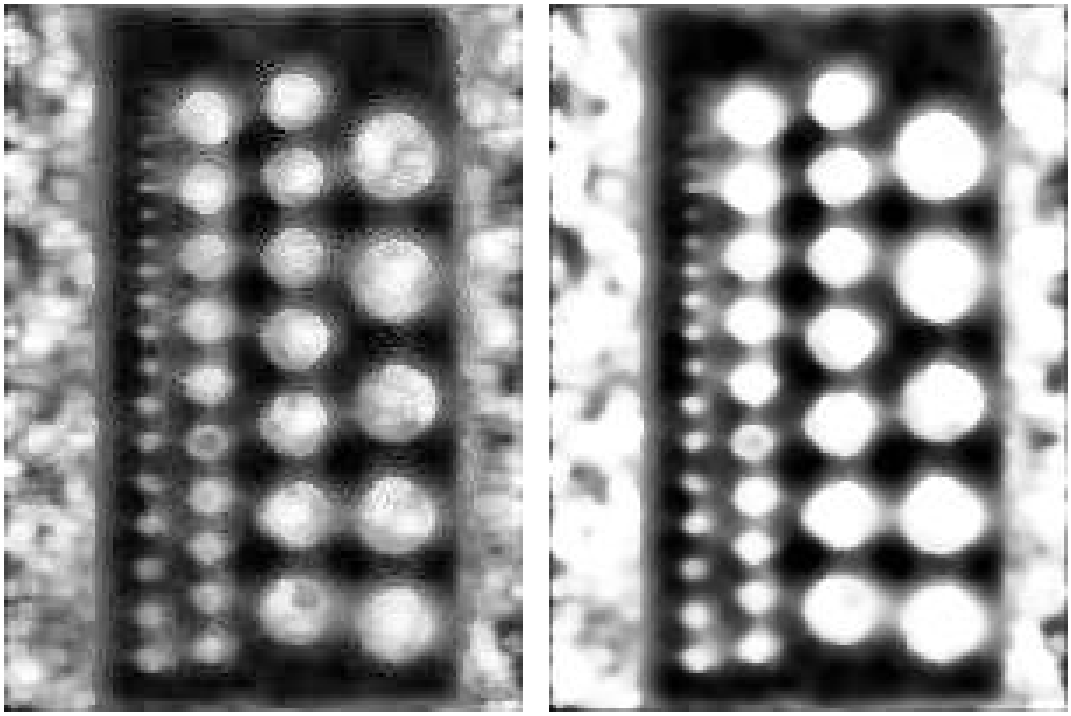

Figure 4.14: Contrast adjustment. Left: result of adaptive histogram equalization, right: adaptive histogram equalization followed by ultra filter

4.2.6 Adaptive Morphological Operator

Another interesting method that uses erosion and dilation is the adaptive morphological operator. This method uses fuzzy techniques to switch between these two functions, as it was explained in section 3.4.2. The result of this method is shown in Fig. 4.15 and the combination of adaptive morphological operator with ultra filter is shown as well.

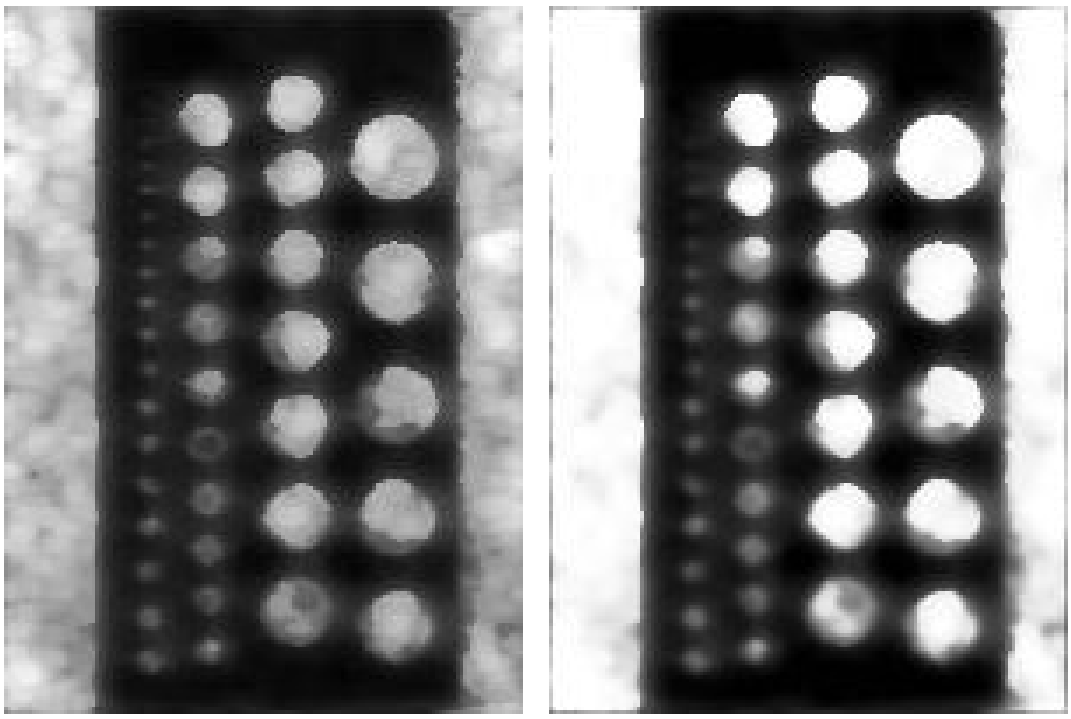

Figure 4.15: Morphological processing. Left: Result of fuzzy morphological operator, right: fuzzy morphological operator followed by ultra filter

4.2.7 Local Adaptive Otsu

The Otsu method calculates a global threshold that converts the intensity image to a binary image by selecting a threshold to minimize the interclass variance of the black and white pixels [50] . However, after using this method, the result were not satisfactory to be presented in this thesis. Therefore, locally adaptive Otsu method was developed. Table 4.2 presents this algorithm.

4.2.8 Segmentation Results

In this section, the segmentation results of the pre-processing methods are presented by using two different segmentation methods; Local adaptive Otsu, and K-means clustering. Windows of size 18×18 were selected for the local adaptive Otsu, and two classes of white and black were set for the K-means clustering. The best results were capture by applying a 5 pixels in length, and 2 pixels in width sticks filter, segmented with local adaptive Otsu segmentation. Also, the combination of Frost filter, ultra filter, and K-means clustering delivered good results. For comparison purposes, results of pre-processing methods with different segmentation methods are shown in Fig. 4.16, Fig. 4.17, and Fig. 4.18, and Fig. 4.19.

As it was mentioned in previous chapter, longer sticks achieve better line enhancement with less noise reduction. However wider sticks are more sensitive to noise with dimmer boundaries. This is very apparent in Fig. 4.16, and Fig. 4.17. More noise was reduced when the width was 2 pixels for sticks filter and a shorter stick. As a result, better segmentation was achieved, and more circles were detected. Also, in this example local adaptive Otsu had much better results than K-menas clustering.

In addition, the result of Frost filter and Frost with ultra filter were not significantly different. This proves that stronger noise reduction and adaptive contrast adjustment were not very effective in this case. When local adaptive Otsu was applied many circles were detected. However, the shape of the circles were not exact and many of them could not be classified as circles (subjective to viewers opinion). While K-means algorithm in this case

Table 4.2: Local Adaptive Otsu

Determine the image size $[R, C]$

Determine the window size n

Determine the window step= $floor(n/2)$

Determine the window overlap= $floor(n/2)$

Initialize counters $rr = 1$, $cc = 1$

for i=step+1:overlapp:R-step

  for j=step+1:overlapp:C-step

    sub=I(i-step:i+step,j-step:j+step);

    Find $T(rr, cc)$ for the sub-image using the Otsu method

    $cc = cc + 1$;

    if $j + n - 2 > C - step$

      $cc = 1$;

    end

  end

  rr=rr+1;

  if $i + n - 2 > R - step$

    $rr = 1$;

  end

end

Resize T to size $[R, C]$ (interpolation)

Threshold all pixels using corresponding threshold

detected more circles when Frost and ultra were combined.

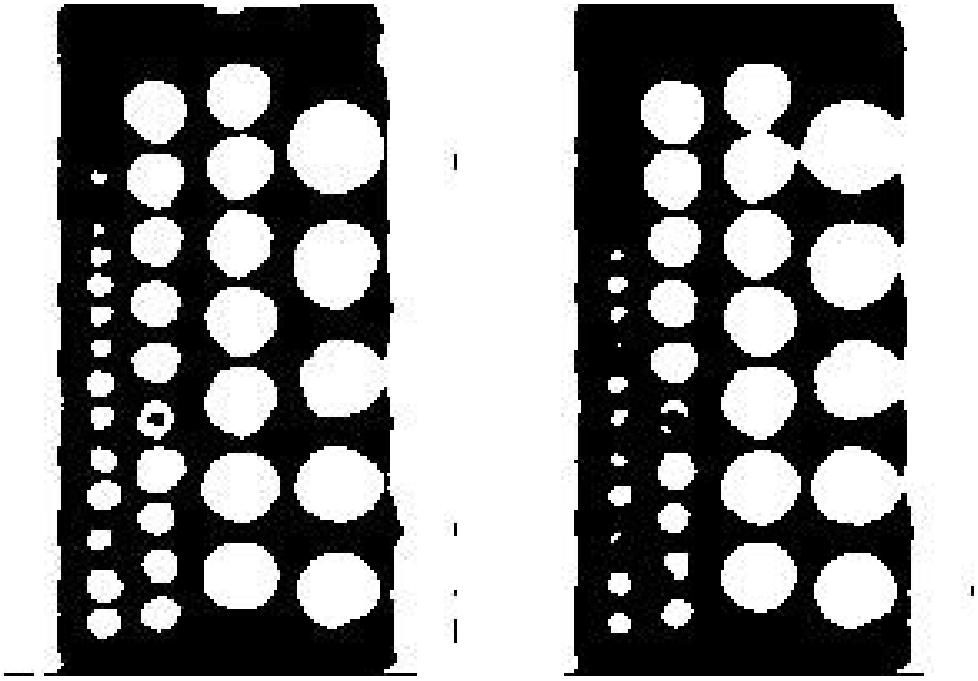

Figure 4.16: Result of sticks filter ($l = 5, w = 2$). Left: segmented via local adaptive Otsu, right: segmented via K-means clustering

Table 4.3 displays the detection accuracy of the images above. The most accurate detection method, as it would be called case 1, was the combination of sticks ($l = 5, w = 2$), and local adaptive Otsu. This method detected the circles with 83% accuracy. This number is the number of circles detected by using this technique divided by the total number of circles. However, the number of circles detected is subjective. The second best results, in terms of more complete circles and good detection accuracy was achieved by using Frost and ultra filters with K-means clustering with detection accuracy of 58%. This would be named case 2 in this section.

To find out how accurately the circles were detected, the detection error between the diameters of the real circles and the diameters of the circles in the image was evaluated. A simple method was proposed: By measuring the length of the phantom in the original image (assumption: the most accurate part in the image), and comparing it to the real length of

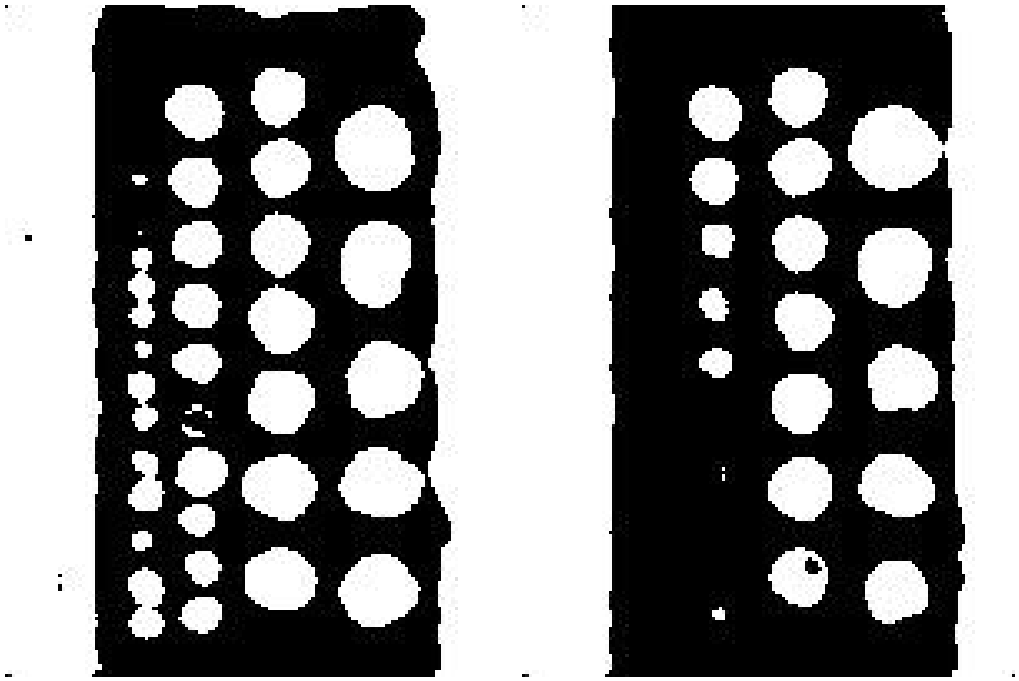

Figure 4.17: Result of sticks filter ($l = 7, w = 1$). Left: segmented via local adaptive Otsu, right: segmented via K-means clustering

the phantom, the resolution, the number of dots per inch (DPI), was calculated. The DPI is 25 pixels per inch. After evaluating the DPI, four different diameters of each circle were measured manually by using tools in Matlab. The vertical, horizontal, and two diagonals were considered. Then, the average of the four was determined. Equation 4.5 determines the calculated diameter in inches:

$$\text{Calculated Diameter} = \frac{\text{average of four different diameters (pixels)}}{\text{DPI (pixels/inches)}} \tag{4.5}$$

This method was applied to case 1 and case 2. Table 4.4, and Table 4.5 show the measurement of sticks filter ($l = 5, w = 2$) and local adaptive Otsu. Table 4.6, and Table 4.7 display Frost, ultra filters and K-menas clustering. By observing the numbers one can see the visual and analytical results match.

The average and standard deviation of error for case 1 and 2 are displayed in Table 4.8. By observing the table, one can see that the average error between the calculated diameters

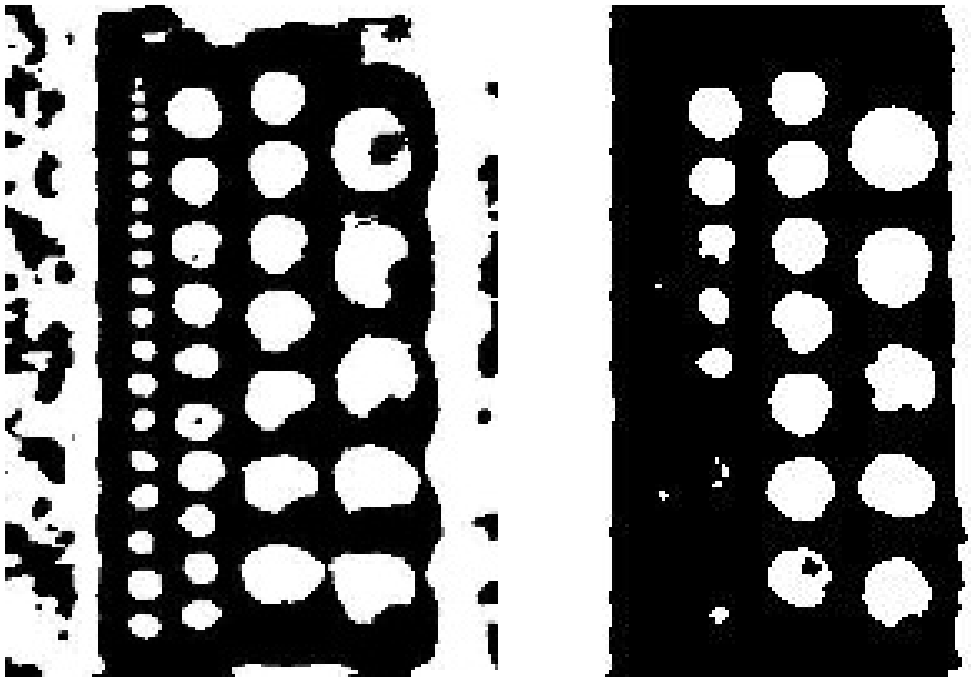

Figure 4.18: Result of Frost filter. Left: segmented via local adaptive Otsu, right: segmented via K-means clustering

and the real diameters are quite low. For case 1 the circles were detected with an average error of 0.117 and standard deviation of 0.213, with 83 % accuracy detection. In case 2, a very low average error of 0.078, with standard deviation of 0.069 can be observed, however, with an accuracy detection of 61%.

After observing and analyzing all the results after pre-processing techniques and segmentation methods, it was obtained that preferred pre-procssing methods for the segmentation accuracy measurements is sticks filter with l=5 and w=2, combined with developed local adaptive Otsu. By increasing the width of the sticks filter, better noise reduction is attained. Also, by reducing the length of the sticks filter the boundaries are dimmer for better noise reduction. However, by applying a local adaptive segmentation method with the ability to capture the spatial information more accurately, this problem can be fixed and the boundaries can be detected with higher precision. These results are very encouraging due to novelty of this technology and lack of information on THz imaging in literature.

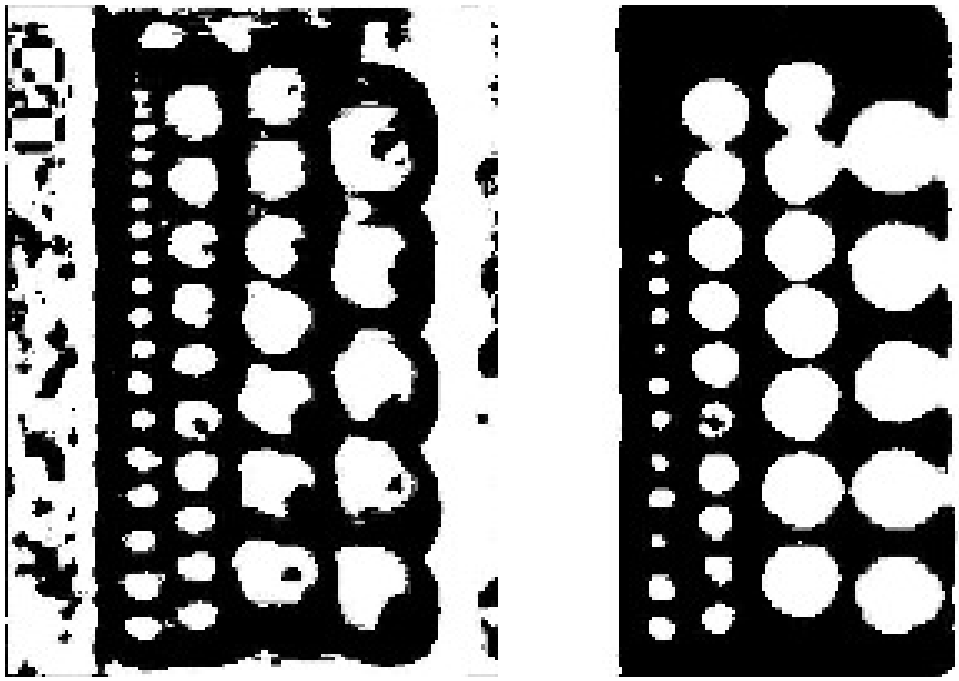

Figure 4.19: Result of Frost filter and ultra filter. Left: segmented via local adaptive Otsu, right: segmented via K-means clustering

4.2.9 Summary

In this chapter proposed algorithms, and algorithms discussed in chapter 3 were applied on the samples. First, images of composite materials which are used in aerospace industry were tested for defect detection. It was observed that the penetration through this type of composite material is only possible in a specific window of frequencies, and the penetration depth was limited for the purpose of reliable defect detection. Second, a phantom sample was examined under THz radiation for accuracy measurements. The most accurate detection method was the combination of sticks ($l = 5, w = 2$), and local adaptive Otsu. This method detected the circles with 83% accuracy. In spite of the immense potentials of the THz technology, practical obstacles seem to be still dominant such that future hard- and software developments should shed more light on the encountered problems and hopefully solve some of them in the near future.

Table 4.3: The ratio of detected circles to total number of existing circles in the phantom image for different pre-processing and segmentation methods

Preprocessing	Segmentation	Detection Accuracy
Sticks (l=7, w=1)	Local Adaptive Otsu	23/41=0.56
Sticks (l=7, w=1)	K-meas	17/41=0.41
Stick (l=5, w=2)	Local Adaptive Otsu	34/41=0.83
Stick (l=5, w=2)	K=means	24/41=0.58
Frost	Local Adaptive Otsu	30/41=0.73
Frost	K-means	15/41=0.37
Frost & Ultra	Local Adaptive Otsu	22/41=0.54
Frost & Ultra	K-menas	25/41=0.61

Table 4.4: Error of the calculated diameters for case 1, [The first three columns of the circles]

Real Size (inches)	Average of Four Diameters (pixels)	Calculated Diameter (inches)	Error
1	27.595	1.100	0.100
0.969	25.042	1.002	0.033
0.938	N/A	N/A	N/A
0.906	23.315	0.933	0.027
0.875	22.923	0.917	0.042
0.844	21.690	0.868	0.024
0.812	22.510	0.900	0.088
0.781	20.710	0.828	0.470
0.750	20.248	0.810	0.06
0.719	18.645	0.746	0.027
0.688	18.987	0.759	0.071
0.656	18.965	0.759	0.103
0.625	18.458	0.738	0.113
0.594	16.575	0.663	0.069
0.562	16.228	0.649	0.870
0.531	13.875	0.555	0.024
0.500	12.955	0.518	0.018
0.469	10.720	0.429	0.040
0.438	14.22	0.569	0.131
0.406	10.065	0.403	0.003
0.375	9.978	0.399	0.240
0.359	10.415	0.417	0.058

Table 4.5: Error of the calculated diameters for case 1, [The fourth column of the circles]

Real Size (inches)	Average of Four Diameters (pixels)	Calculated Diameter (pixels/inches)	Error
0.344	9.448	0.378	0.034
0.328	9.855	0.394	0.066
0.312	6.545	0.262	0.050
0.297	9.278	0.371	0.074
0.281	7.508	0.300	0.019
0.266	7.070	0.283	0.017
0.250	7.563	0.303	0.053
0.234	5.273	0.211	0.023
0.219	6.293	0.252	0.033
0.203	7.345	0.294	0.910
0.188	5.87	0.235	0.047
0.172	3.733	0.149	0.023
0.156	N/A	N/A	N/A
0.141	3.820	0.153	0.012
0.125	N/A	N/A	N/A
0.109	N/A	N/A	N/A
0.094	N/A	N/A	N/A
0.078	N/A	N/A	N/A
0.0.62	N/A	N/A	N/A

Table 4.6: Error of the calculated diameters for case 2, [The first three columns of the circles]

Real Size (inches)	Average of Four Diameters (pixels)	Calculated Diameter (pixels/inches)	Error
1	N/A	N/A	N/A
0.969	N/A	N/A	N/A
0.938	N/A	N/A	N/A
0.906	N/A	N/A	N/A
0.875	23.895	0.9558	0.081
0.844	22.6675	0.9067	0.063
0.812	22.933	0.9173	0.105
0.781	21.560	0.8624	0.081
0.750	20.985	0.8394	0.089
0.719	20.223	0.809	0.090
0.688	N/A	N/A	N/A
0.656	N/A	N/A	N/A
0.625	N/A	N/A	N/A
0.594	N/A	N/A	N/A
0.562	15.508	0.6203	0.058
0.531	14.208	0.5683	0.037
0.500	13.525	0.541	0.041
0.469	N/A	N/A	N/A
0.438	11.470	0.4588	0.010
0.406	9.350	0.374	0.064
0.375	8.075	0.323	0.083
0.359	8.403	0.3361	0.039

Table 4.7: Error of the calculated diameters for case 2, [The fourth column of the circles]

Real Size (inches)	Average of Four Diameters (pixels)	Calculated Diameter (inches)	Error
0.344	6.790	0.272	0.072
0.328	7.425	0.297	0.031
0.312	3.850	0.154	0.158
0.297	6.773	0.271	0.026
0.281	4.5825	0.183	0.098
0.266	5.255	0.210	0.056
0.250	5.208	0.208	0.042
0.234	4.838	0.196	0.0405
0.219	5.498	0.220	0.001
0.203	3.605	0.144	0.145
0.188	N/A	N/A	N/A
0.172	N/A	N/A	N/A
0.156	N/A	N/A	N/A
0.141	1.453	0.0581	0.083
0.125	N/A	N/A	N/A
0.109	N/A	N/A	N/A
0.094	N/A	N/A	N/A
0.078	N/A	N/A	N/A
0.0.62	N/A	N/A	N/A

Table 4.8: Average and standard deviation of error for conducted measurements

	Case 1	Case 2
Average	0.117	0.078
Stdev	0.213	0.069

Chapter 5

Summary and Conclusions

THz imaging era has begun after Hu and Nass have developed the first real time imaging system in 1995. This endeavor commenced new opportunities in many applications such as quality control, security, biomedical diagnosis etc. The fact that this type of testing is non-destructive and contact-free puts this technology ahead of some existing technologies of x-ray and thermal imaging specially if we remember the unique characteristics of THz waves and how they interact with matter.

Due to the distinct characteristics of the T-rays, Terahertz images can provide significant information about the internal structures of materials. These radiation can penetrate trough most dielectrics; paper, plastic, leather, wood. However, in this thesis for the first time composite material, which are used in the aerospace industry were under examination. The imaging of this material is extremely challenging since penetration is limited. Also, segmentation accuracy of THz images were under testing by using a phantom with 41 different circles inside of two cardboards. This material is transparent under THz waves with the output power of 181 mW at 1.63 THz.

After comprehensive research, continuous gas laser was depicted over THz pulsed imaging system. This was due to the fact that this type of imaging has higher power spectral density, in other words better image resolution. Also, among continuous systems gas lasers can achieve higher output power than other technologies such as photomixing of two diode lasers.

In addition, they are more cost effective compared to other alternatives such as quantum cascaded lasers.

Nevertheless, due to novelty of this technology image processing techniques customized for THz images have been widely ignored in literature. Image segmentation is a difficult task especially for Terahertz images. Therefore, using intelligent pre-processing methods before the actual segmentation could improve the result significantly. In this work, methods that are applied for ultrasound images have been employed. Also many techniques were developed by using fuzzy image processing to be able to pre-process the images before segmentation.

Methods such as sticks filter, Frost filter, fusion of median and Wiener filters, fuzzy contrast adjustment, fusion of phase and amplitude images have achieved promising results in this work. Sticks filter is a strong edge preserving filter, which diminished the noise quite successfully in both experiments. In addition, by fusing phase and amplitude images using fuzzy techniques best information in both images were obtained. After this step, a simple segmentation method located the defect.

Another encouraging result is the combination of Frost filter with ultra filter (fusion of median and wiener filter with a fuzzy contrast adjustment). This method was able to subside the noise level, therefore simple k-means clustering was able to segment the image.

The future works should concentrate on more sophisticated approaches for filtering and fusion of Terahertz images. Furthermore, due to time-consuming nature of THz image acquisition the number of images in this thesis was limited. In the future, with more data available due to rapid advancement in this technology, a larger variety of soft computing techniques could be applied on the images. For instance, methods such as neural networks could be useful. Also, noise identification for THz images is essential. By modeling the noise type, scientists will know how to reduce that particular type of noise.

The growth of the Terahertz technology for the past 13 years have been astonishing, and with the same rate of growth this technology is very auspicious in near future.

Bibliography

[1] J. Handley; "Time Frequency Analysis Techniques in Terahertz Pulsed Imaging". A PhD thesis, University of Leeds School of Computing, Dec. 2003

[2] D.M. Mittleman, "Sensing with Terahertz Radiation", Springer, 2003

[3] D. Dragoman, M.Dragoman; "Terahertz Fields and Applications", Progress in Quantum Electronics. pp. 1-66, 2004

[4] D. Mittleman; M. Gupta; R. Neelamani; R.G Baraniuk; J.V Rudd; M. Koch; "Recent Advances in Terahertz Imaging", Applid Physics B 68, Lasers and Optics, pp. 1085-1094, 1999

[5] B. B Hu; M.C Nuss, "Imaging with terahertz waves, OPt. Lett. 20, pp.1716-1718, 1995

[6] D.M. Mittelman; J. Cunningham; M.C Nuss; M. Geva; "Non contact Semi Conductor Wager Characterization with the Terahertz Hall Effect", Appl. Phys. lett. 71, pp. 16, 1997

[7] M. Brucherseifer; P. Haring Bolivar; H. Klingenerg; H. Kurz; "Angle Dependent THz Tomography Characterization of Thin Ceramic Oxide Films for Fuel Cell Applications", Appl. Phys. B 72,pp. 361, 2001

[8] M. Shur; "Terahertz technology: devices and applications", Solid-State Circuits Conference, pp. 13-21, 12-16 Sept. 2005

[9] H. Rubens; E.F Nichols; "Heat rays of great wavelength", Physics Review, pp. 314-323, 1897

[10] M. J. Warmuth; "PAT in Manufacturing/QA An Industry Perspective", American Pharmaceut. Rev Magazine, Fall 2003

[11] C.F. Bohren; D. Huffman; "Absorption and scattering of light by small particles", John Wiley, New York, 1983

[12] H. Zhong; A. R. Sanchez; X.-C. Zhang "Identification and classification of chemicals using terahertz reflective spectroscopic focal plane imaging system", Volume 14, No. 20, Optics Express, 9130, October 2006

[13] H-B Liu; H. Zhong; N. Karpowicz; Y. Chen; X-C Zhang; "Terahertz Spectroscopy and Imaging for Defense and Security Applications", Proceedings of the IEEE, Volume 95, Issue 8, pp. 1514-1527, Aug. 2007

[14] M. Koch; "THz-Imaging: Fundamentals and Biological Applications", EUROPTO conference on Terahertz Spectroscopy, SPIE vol. 3828, pp.202-208, June 1999

[15] Y.R Shen; " Far-infrared generation by optical mixing", prog. Quantum Electron 4, 207, 1976

[16] M. van Exter; D. Grishchkowsky; "Characterization of and Optoelectric Terahertz Beam System", IEEE Trans. on Microwave Theory and Techniques, 38, pp. 1684-1691, 1990

[17] J. V. Rudd; D. Zimdars; M. Warmuth; "Compact, Fiber-pigtailed Terahertz Imaging System", Proc. SPIE 3934, 27, 2000

[18] T. Kleine-Ostmann; P. knobloch; M. Koch, S. Hoffmann, M. Breede; M. Hofmann; G Hein; K. Pierz; M. Sperling; K. Donhuijsen; "Continuous-wave THz Imaging" Electronics letters, 37(24), pp. 1461-1463, 2001

[19] K.J Siebert; H. Quast; R. Leonardt; T Lffler; M. Thomson; T. Bauer; H.G. Roskos "Continuous-wave all-aptoelectric Terahertz Imaging" Applied Phys. letters, 80(16), pp.3003-3005, April 2002

[20] K. J. Siebert; T. Lffler; H. Quast; M. Thomson; T. Bauer; R. Leonhardt; S. Czasch; H. G. Roskos; "All- optoelectronic Continuous wave THz Imaging for Biomedical Applications, Phys. Med. Biol., 47, pp. 3743- 3748, 2002

[21] I. Hosako; N. Sekine; M. Patrashin; S. Saito; K. Fukunaga; Y. Kasai; P. Baron; T. Seta; J. Mendrok; S. Ochiai; H. Yasuda; "At the Dawn of a New Era in Terahertz Technology", Proceedings of the IEEE, Volume 95, Issue 8, pp. 1611 - 1623, Aug 2007

[22] B. S. Williams; S. Kumar; H. Qing; J. L. Reno; "Operation of terahertz quantum-cascade lasers at 164 K in pulsed mode and at 117 K in continuous-wave mode", Optics Express, Volume 12. No. 9, pp. 3331, May 2005

[23] R. Kohler; A. Tredicucci; F. Beltram; H. E. Beere; E. H. Lineld; A. G. Davies; D. A. Ritchie; R. C. Iotti; F. Rossi; "Terahertz semiconductor-heterostructure laser, Nature 417, pp. 156, 2002

[24] P. Und Jespen; R.H. Jacobson; S.R. keiding; J. OPt. Soc. Am, B, 13, pp. 2024, 1996

[25] I. S. Gregory; T.D Drysdale; W.R Tribe; D.R.S. Cumming; M.J Evans; M. Missous; E.H. Linfield; "Multichannel Continuous-Wave Terahertz Imaging, Infrared and Millimeter Waves", 2004

[26] V.P. Wallace; D.A. Arnone; R.M. Woodward; R.J. Pye; "Biomedical Application of Terahertz Pulsed Imaging", Proceedings of the Second Joint Volume 3, pp. 23-26 Oct. 2002

[27] D.M. Mittleman; R.H Jacobsen; M.C. Nuss; "T-ray imaging", Selected Topics in Quantum Electronics, IEEE Journal of Volume 2, Issue 3, pp. 679 - 692, Sep. 1996

[28] D.M. Mittleman.; R. Neelamani; R.G Baraniuk; M.C. Nuss; "Applications of terahertz imaging", Nonlinear Optics, pp. 294-296 Aug. 1998

[29] J. Darmo, V. Tamosiunas, G. Fasching, J. Krll, K. Unterrainer, M. Beck, M. Giovannini, J. Faist, C. Kremser; P. Debbage, "Imaging with a Terahertz quantum cascade laser", Opt. Express 12, pp. 1879-1884 , April 2004

[30] I. S. Gregory; W. R. Tribe; B. E. Coleb; C. Bakera; M. J. Evansb; I. V. Bradleyb; E. H. Linfielda; A. G. Daviesa; M. Missousc; "Continuous-wave terahertz imaging using diode lasers"; SPIE Optics, Volume 5354, 2004

[31] S. Gregory; W. R. Tribel; L. Spence; V. P. Wallace; "Multichannel Continuous-Wave Terahertz Imaging",IEEE Trans, 13th intl. Conf on Terahertz Electronics, pp. 46-47, 2005

[32] R. F. Kazarinov; R. A. Suris; "Possibility of amplification of electromagnetic waves in a semiconductor with superlattice", Sov. Phys. Semi cond. , Volumel 5, pp.707709, 1971

[33] J. Faist; F. Capasso; D. L. Sivco; C. Sirtori; A. L. Hutchinson; A. Y. Cho; "Quantum cascade lasers", Science, Volume 264, pp. 553556, 1994

[34] L.A Zadeh; "A theory of approximate reasoning" Machine Intelligence, Volume 9, pp.149-94, Elsevier, New York, 1979

[35] S.K Pal; D.D. Madjumadar;"Fuzzy Mathematical Approach to Pattern Recognition", 1986

[36] J.C. Bezdek, S.K Pal, "Fuzzy Models for Pattern Recognition", Bezdek, 1992

[37] F.O. Karray, C. deSilva; "Soft Computing and Intelligent System Design, Theory Tools and Application", Pearson Addison Wesley, 2004

[38] H.R Tizhoosh; Fuzzy Image Processing: "Introduction in Theory and Applications", Springer-Verlag , Germany, 1997

[39] H.R Tizhoosh; M.Fochem; “Image Enhancement with Fuzzy Histogram Hyperbolization”. In: Proceedings von EUFIT95, Volume 3, pp. 1695-1698, 1995

[40] R.N. Czerwinski; “Line and boundary detection in speckle images, IEEE Trans. Image Processing, Volume 7, pp. 17001714, Dec. 1998

[41] R.N. Czerwinski; “Detection of Lines and Boundaries in Speckle ImagesApplication to Medical Ultrasound”, IEEE Trans. on medical imaging, Volume 18, no.2, February 1999

[42] Y. Yongjian; S.T. Acton; “Speckle reducing anisotropic diffusion”,Volume 11,Issue 11, pp. 1260 - 1270, Nov. 2002

[43] N. Wienre; “Extrapolation, Interpolation, and Smoothing of Stationary Time Series”, New York, 1949

[44] F. Jin; P. Fieguth; L. Winger; E. Jernigan; “Adaptive Wiener filtering of noisy images and image sequences”, International Conference on Image Processing, Volume 3, Issue 14-17, pp. III - 349-52 vol.2, Sept. 2003

[45] G.A. Baxes.; “Digital Image Processing. Principles & Applications, Wiley & Sons, 1994

[46] X. Zhuang; R.M. Haralick; “Morphological Structural Element Decomposition”, CVGIP(35), No. 3, pp. 370-382, September 1986

[47] J.Theiler; G. Gisler; “A contiguity-enhanced k-means clustering algorithm for unsupervised multispectral image segmentation”, Proc SPIE 3159. pp. 108–118, 1997

[48] R.C Gonzales; R.E Woods; “Digital Image Processing”, Prentie Hall, New Jersy, U.S.A, 2002

[49] M.S. Aldenderfer, R.K. Blasheld, “Cluster Analysis”, Sage Publications,Thousand Oaks, California, U.S.A, 1984

[50] N. Otsu, “A Threshold Selection Method from Gray-Level Histograms,” IEEE Transactions on Systems, Man, and Cybernetics, Volume 9, No. 1, pp. 62-66, 1979